NASA Technical Memorandum 80212

Theoretical Study of Nonadiabatic Boundary-Layer Stabilization Times in a Cryogenic Wind Tunnel for Typical Stainless-Steel Wing and Fuselage Models

Charles B. Johnson

JULY 1980

NASA

NASA Technical Memorandum 80212

Theoretical Study of Nonadiabatic Boundary-Layer Stabilization Times in a Cryogenic Wind Tunnel for Typical Stainless-Steel Wing and Fuselage Models

Charles B. Johnson
Langley Research Center
Hampton, Virginia

National Aeronautics
and Space Administration

**Scientific and Technical
Information Office**

1980

SUMMARY

A theoretical study has been made of the effect of nonadiabatic wall conditions on boundary-layer properties for 4 stainless-steel model configurations at stagnation pressures of 2, 6, and 9 atm. The purpose of the analysis is to determine the time required for typical models to reach an adiabatic wall condition after a 50-K step change in total temperature. A transient-conduction analysis is coupled with a boundary-layer analysis to give stabilization times for various model configurations and tunnel conditions. The model configurations include a solid NACA 0012-64 airfoil and three bodies of revolution (one solid and two hollow with varying wall thicknesses). The models are representative of the wing root chord and fuselage of a typical transport model for the National Transonic Facility. The results showed that the time to reach an adiabatic wall condition following a 50-K step change in total temperature varies from slightly more than 10 min to 1.5 min, depending on the configuration and stagnation pressure. The maximum error in boundary-layer properties for a 50-K step change in total temperature is between 12 and 13 percent for the local skin friction and between 25 and 29 percent for the displacement thickness. The initial error in boundary-layer properties decreases very rapidly with time and the maximum error is reduced to 50 percent of its initial value in a short period of time; however, due to the nonlinearity of the cooling process the time to reach an adiabatic condition is approximately 25 times longer than the time to reach the 50-percent reduction in error condition. The time to reach an adiabatic condition decreases significantly with an increase in stagnation pressure and, as would be expected, reducing the mass of the model also significantly reduces the time to reach an adiabatic condition.

INTRODUCTION

The most technologically advanced cryogenic wind tunnel is the National Transonic Facility (NTF) which is now being constructed at the NASA Langley Research Center (refs. 1 to 3). By being able to vary total temperature independently of total pressure, this cryogenic wind tunnel will offer the advantage of testing over a greatly increased range of Reynolds numbers while avoiding many of the practical problems that would be associated with testing at high Reynolds numbers in conventional ambient-temperature—high-pressure tunnels.

From the standpoint of operational flexibility and economy, it is desirable to change the Reynolds number rapidly during a given test by a very rapid change in total temperature. After a rapid change in total temperature the model will not be in thermal equilibrium with respect to the free stream but will, over a period of time, be cooling (or heating) toward its adiabatic wall condition. In order to determine the usefulness of the ability to make the very rapid change in total temperature for aerodynamic testing, a theoretical conduction analysis has been made to determine the time it takes a typical NTF transport model to reach an adiabatic wall condition following a large step change in total temper-

ature. In addition, the conduction analysis was combined with a boundary-layer analysis to determine the effect of a nonadiabatic wall on the boundary-layer properties. The results of this study are presented herein.

SYMBOLS

C_f local skin-friction coefficient, $\dfrac{\tau}{\frac{1}{2}\rho_e u_e^2}$

C_p pressure coefficient, $\dfrac{p - p_\infty}{q_\infty}$

c chord of NACA 0012-64 airfoil, 25.4 cm

$\bar{c}$ mean geometric chord, 25.0 cm

c_p specific heat

h heat-transfer coefficient

k thermal conductivity

L length of NASA body of revolution, 121.92 cm

M Mach number

p pressure

q dynamic pressure

$R_{\bar{c}}$ Reynolds number, based on $\bar{c}$

T temperature

t time

u velocity

x distance along chord of airfoil or center line of body of revolution

α angle of attack

ΔT step change in total temperature

δ^* boundary-layer displacement thickness

ρ density

τ model skin thickness

Subscripts:

aw adiabatic wall conditions

e edge of boundary layer

i initial conditions

max maximum

min minimum

s surface conditions

t stagnation (or total) conditions

w wall condition

∞ free-stream conditions

BASIS FOR ANALYSIS

It is well known that one of the major testing advantages of cryogenic wind tunnels is the expanded operating envelope resulting from the ability to vary T_t as well as p_t. This advantage is illustrated in figure 1(a) which shows a typical operating envelope for the NTF at a test section Mach number of 0.8. The upper boundary of the operating envelope is set by a maximum operating pressure of 9 atm (1 atm = 101.3 kPa) which is based on the structural limit of the pressure shell. The lower boundary of the operating envelope is set by the need to operate at a pressure slightly greater than atmospheric pressure in order to vent nitrogen gas when using liquid nitrogen to cool the tunnel. The boundary on the left is determined by the maximum T_t, which is about 340 K, coupled with the restraints dictated by the fan drive system. The boundary on the right is determined by the minimum T_t that will avoid local saturation (condensation) over the model which for $M = 1.4$ and $p_t = 6.65$ atm is about 117 K. T_t based on the $M = 1.4$ saturation boundary varies from 96 K at the minimum pressure (atmospheric) to 122 K at the maximum pressure. The operating characteristics of pressurized cryogenic tunnels, such as the NTF, make possible the unique testing capability of pure Reynolds number studies at a constant pressure by the appropriate changes in T_t, as indicated by the horizontal line in figure 1(a). Also, pure aeroelastic studies at a constant Reynolds number (as indicated by the vertical line in fig. 1(a)) can be obtained by varying p_t with an appropriate adjustment of T_t. The variation of Reynolds number with temperature as indicated in reference 4 is nonlinear, with the greatest change in Reynolds number per unit temperature change occurring at the lowest temperature. Therefore, the present analysis was made for a ΔT of 50 K between temperatures of 167 K and 117 K (near minimum temperature) which corresponds to a Reynolds number range for the NTF from 50×10^6 to 85×10^6 at 6.65 atm as indicated in figure 1(b).

In this phase of the investigation a step change in temperature was assumed. This gives a somewhat optimistic estimate of the time required for the model to reach adiabatic conditions. The actual time required to make a 50-K step change in the NTF was not known at the time of this analysis, however, it is estimated to be on the order of 15 to 30 sec at pressures of 2 to 6 atm. A rapid decrease in T_t means that the recovery temperature of the flow will be less than the temperature of the model and that for a period of time the model will be cooling toward its adiabatic wall temperature. The consequent heat transfer will significantly affect the boundary-layer properties until the adiabatic wall condition is reached. As noted in reference 4, results from boundary-layer calculations made at a flight Reynolds number show that if an ideal-gas method of calculation (i.e., flight calculations) is compared to a real-gas cryogenic method of calculation (i.e., NTF application) there is virtually no difference in boundary-layer properties if both the results are at adiabatic wall conditions. The analysis made in this report will examine local skin friction C_f and boundary-layer displacement thickness δ^* from the time the total temperature is changed until the time the model reaches an adiabatic wall condition. These two parameters (C_f and δ^*) were chosen because they are two basic viscous boundary-layer characteristics used in inviscid and viscous wind-tunnel simulation. For all of the conduction calculations presented herein, it is assumed that a 50-K step change in total temperature from 167 K to 117 K occurs at $t = 0$.

METHOD OF ANALYSIS

This report presents results from a theoretical study of the time-varying effects of nonadiabatic wall conditions on boundary-layer properties for two hypothetical model configurations made from AISI type 310S stainless steel. The geometry used in the conduction analysis for wing and fuselage simulation are shown in figure 2 in relation to a wind-tunnel model sized for use in the NTF. The root section of the wing is simulated by the NACA 0012-64 airfoil with a 25.4-cm chord. The fuselage is simulated by a NASA body of revolution, referred to in reference 5 as body 11, with a length of 121.92 cm and a thickness-to-length ratio of about 0.105. The geometry of the four configurations that were analyzed is shown in figure 3. The NACA 0012-64 airfoil was input into the conduction code as a solid body. The body of revolution was analyzed as a solid body, a body with a 2.54-cm-thick wall, and a body with a 1.27-cm-thick wall. The pressure distributions that were used as input for all boundary-layer calculations are shown for the airfoil and the body of revolution in figures 4 and 5, respectively. The pressure distribution over the airfoil, found in reference 6, was obtained at cryogenic conditions. The pressure distribution over the body of revolution (ref. 5) was obtained at room temperature conditions.

The six steps used in the method of analysis are:

1. Determine heating rates for the airfoil section and the body of revolution at $M_\infty \approx 0.85$ and $\alpha = 0^\circ$ using measured pressures.

2. Determine effect of T_w/T_t ratio and p_t on heating of bodies.

3. Discretize the two-dimensional airfoil and body of revolution into conduction and storage nodes.

4. Input heat-transfer coefficients and nodal geometry into transient heat conduction code and determine temperature history for 310S stainless steel with step changes in total temperature at $t = 0$.

5. Make boundary-layer calculations for various T_w/T_t ratios over a range of T_t and p_t for the airfoil and the body of revolution.

6. Evaluate error in boundary-layer properties, relative to adiabatic conditions, due to nonadiabatic wall conditions by combining results of steps 4 and 5. Subsequent sections of this paper describe in detail each of the six steps in the analysis and give results in terms of the stabilization times for skin friction and boundary-layer displacement thickness.

RESULTS AND DISCUSSION

Boundary-Layer Calculations

The effect of p_t and the T_w/T_t ratio on the heat-transfer coefficient h calculated by the method in reference 7 is shown in figure 6 for a station on the NACA 0012-64 airfoil. The usual large effect of p_t on the level of h is indicated. A similar effect of the T_w/T_t ratio and p_t was observed for the body of revolution. The conduction code used a constant distribution of h in its solution. Thus, the distribution of h was calculated at a mean value of $T_w/T_t = 1.22$ to give an approximation of the time-varying value of T_w/T_t. The value of $T_w/T_t = 1.22$ falls midway between the initial value of 1.41 and the final (i.e., adiabatic) value of about 0.985. For stagnation pressures of 2, 6, and 9 atm the distribution of h over the airfoil and the body of revolution is shown in figures 7 and 8, respectively. The distributions of h were used as input for the heat conduction analysis. At $p_t = 2$ atm the beginning of transition was assumed to be about 3 and 4 percent of chord (and length) for the airfoil and the body of revolution, respectively. For the higher pressures the start of transition moves upstream as would be expected due to the increased Reynolds number. For both the airfoil and the body of revolution the material used in the conduction analysis was 310S stainless steel. The physical properties used in the conduction analysis for 310S stainless steel are given in table I.

TABLE I.- PHYSICAL PROPERTIES FOR 310S STAINLESS STEEL

[ρ = 8027.0 kg/m^3]

Physical property	Values of physical properties at temperatures, K, of -				
	373.3	273.0	200.0	100.0	50.0
c_p, J/kg-K	502.0	480.0	415.0	255.0	105.0
k, W/m-K	13.8	12.4	10.8	8.10^{1}	5.35

The variations of surface temperature with time at three locations on the airfoil are shown in figure 9. The temperature variations were obtained from a computer program, described in reference 8, which uses the backward finite difference method for solving the heat balance equations. As can be seen, the trailing edge of the airfoil, which has a relatively small mass, approaches the adiabatic wall temperature within about 30 sec. The leading edge approaches the adiabatic wall temperature more slowly because of the larger mass in this region compared to the trailing edge. In the region of maximum thickness at the 40-percent chord it takes almost 4 min to reach the adiabatic wall temperature.

The variations of surface temperature with time at three locations on the body of revolution are shown in figure 10. The wall thickness for this particular configuration is 1.27 cm. It can be seen from figure 3 that this configuration has about the same mass per unit surface area at the nose, trailing edge, and midbody. The rate at which these locations approach the adiabatic wall temperature is primarily dependent on the value of h at the respective locations (fig. 8). The recovery temperature ratio T_{aw}/T_t for the airfoil and the body of revolution was 0.985 and 0.990, respectively. The T_{aw}/T_t ratio was held constant over the respective bodies as a requirement of the conduction code. The stagnation point at the nose of the body of revolution has the highest h ($h = 1301$ W/m^2-K) and thus cools rapidly. The midbody station cools somewhat slower than the nose. The trailing edge which has the lowest h cools the slowest. All three stations reach the adiabatic wall temperature at about 240 sec after the 50-K step change in total temperature.

The distribution of surface temperature, over the three configurations of the body of revolution, 30 sec after the 50-K step change in total temperature is shown in figure 11. The peak temperature at $x \approx 5$ cm corresponds to the beginning of transition which is seen in the distribution of h in figure 8. During this period of time, after the 50-K step change in total temperature, the surface-temperature distribution is quite sensitive to the distribution of h over the model. In particular, the location of the beginning and end of transition will strongly affect the temperature distribution over the model. A similar effect was noted for the airfoil.

The $C_f/C_{f,aw}$ ratio is shown in figure 12 as a function of the T_w/T_t ratio at $x/c = 0.4$ on the airfoil. It should be noted that the $C_f/C_{f,aw}$ ratio collapses to a single curve that is nearly independent of p_t and T_t for the range of conditions indicated in figure 12. The skin friction ratios are calculated from a boundary-layer code described in reference 9. The initial wall temperature conditions for which the heat conduction analysis was made correspond to a T_w/T_t ratio of about 1.41 at $t = 0$. At this condition (indicated by the dashed line) C_f is about 88 percent of $C_{f,aw}$ (fig. 12).

The δ^*/δ^*_{aw} ratio is shown in figure 13(a) as a function of the T_w/T_t ratio at $x/c = 0.4$ on the airfoil for $p_t = 2$ atm. The δ^*/δ^*_{aw} ratio forms nearly a single curve for a range of total temperatures from about 333.3 K to cryogenic conditions (83.3 K). In terms of the initial T_w/T_t ratio at $t = 0$ ($T_w/T_t = 1.41$), δ^* is about 26 percent greater than δ^*_{aw}. The data of figures 13(b) and 13(c) are similar to those of figure 13(a) only they are for p_t values of 6 and 9 atm, respectively. The effect of p_t on δ^*/δ^*_{aw} versus

T_w/T_t is shown in figure 14 for the airfoil. Figure 14 is the result of combining the (a), (b), and (c) parts of figure 13. Figure 14 shows the variation of δ^*/δ^*_{aw} as a function of T_w/T_t over the range of T_t from 333.3 K to cryogenic conditions (83.3 K) and over a range of p_t from 2 to 9 atm. The effect of pressure on the δ^*/δ^*_{aw} ratio is indicated in figure 14 by the band of values as the T_w/T_t ratio increases above the adiabatic value.

The $C_f/C_{f,aw}$ ratio is shown in figure 15 as a function of T_w/T_t at the midbody station on the body of revolution. As was noted in figure 12, the $C_f/C_{f,aw}$ ratio collapses to a narrow band that is nearly independent of p_t and T_t for the range of conditions indicated in figure 15. For the initial temperature condition of this study (t = 0), when $T_w/T_t = 1.41$ the local skin friction is about 13 percent below the adiabatic wall value.

The δ^*/δ^*_{aw} ratio is shown in figure 16(a) as a function of the T_w/T_t ratio at the midbody station on the body of revolution for $p_t = 2$ atm. The explanation and results of figure 16(a) is the same as that discussed previously for figure 13(a). For example at $t = 0$ when $T_w/T_t = 1.41$, δ^* is about 13 percent below δ^*_{aw}. The δ^*/δ^*_{aw} versus T_w/T_t curves of figures 16(b) and 16(c) are similar to that of figure 16(a) only they are for p_t values of 6 and 9 atm, respectively. The effect of p_t on δ^*/δ^*_{aw} versus T_w/T_t is shown in figure 17 for the body of revolution. Figure 17 is the result of combining the (a), (b), and (c) parts of figure 16. The variation of δ^*/δ^*_{aw} as a function of T_w/T_t is shown in figure 17 over the range of T_t from 333.3 K to cryogenic conditions (83.3 K) and over a range of p_t from 2 to 9 atm. The effect of p_t on the δ^*/δ^*_{aw} ratio is indicated in figure 17 by the band of values on either side of the adiabatic value of the T_w/T_t ratio.

Boundary-Layer Stabilization Time

The boundary-layer stabilization times due to nonadiabatic wall conditions, as a function of time, are determined by combining the results from the transient heat conduction code, such as shown in figures 9 and 10, with the boundary-layer analysis shown in figures 12 to 16. The results of combining a boundary-layer analysis with the heat conduction results at $x/c = 0.4$ for the airfoil are shown in figures 18 and 19, and at $x/L = 0.5$ for the three shapes of the body of revolution in figures 20 to 25. It should be remembered that the analysis is based on the model being at an initial uniform equilibrium temperature of 164.49 K and then at $t = 0$ there is a 50-K step change in total temperature from 167 K to 117 K. Table II summarizes the stabilization times for the 4 configurations at $M_\infty = 0.85$, for stagnation pressures of 2, 6, and 9 atm. Included in the table is the maximum error (at $t = 0$), the time to reduce the maximum error by 50 percent, the time to reach a condition where the error is 1 percent, and the time to reach an adiabatic condition. The times required for the 4 configurations to reduce the maximum error by 50 percent is considerably less than the times required to reach an adiabatic condition as can be seen in table II. The pronounced increase in the time to reach an adiabatic condition over the time to reduce the maximum error by 50 percent is due to the nonlinearity of the curves in figures 13 to 20. For instance at $t = 0$, the maximum error in boundary-layer properties relative to adiabatic conditions is between

TABLE II.- STABILIZATION TIMES AFTER A 50-K STEP CHANGE IN TOTAL TEMPERATURE

FOR MODELS MADE OF AISI TYPE 310S STAINLESS STEEL

Model configurations	Approximate maximum error, percent	Stabilization times at -								
		p_t = 2 atm			p_t = 6 atm			p_t = 9 atm		
		Time to reduce maximum error by 50 percent, sec	Time to reach a 1-percent error, sec	Time to reach an adiabatic condition, sec	Time to reduce maximum error by 50 percent, sec	Time to reach a 1-percent error, sec	Time to reach an adiabatic condition, sec	Time to reduce maximum error by 50 percent, sec	Time to reach a 1-percent error, sec	Time to reach an adiabatic condition, sec
$C_f/C_{f,aw}$										
NACA 0012-64 (x/c = 0.4)	12	28	142	300	6	72	200	3	55	180
Body of revolution (solid, x/L = 0.5)	13	37	426	>600	9	168	540	6	116	480
Body of revolution (τ = 2.54 cm, x/L = 0.5)	13	36	240	390	9	114	235	5	87	205
Body of revolution (τ = 1.27 cm, x/L = 0.5)	13	29	118	200	8	55	100	5	44	85
δ^*/δ^*_{aw}										
NACA 0012-64 (x/c = 0.4)	26	21	175	300	4	95	200	2	78	180
Body of revolution (solid, x/L = 0.5)	28	29	542	>600	8	262	540	4	193	480
Body of revolution (τ = 2.54 cm, x/L = 0.5)	28	29	289	390	8	150	235	4	120	205
Body of revolution (τ = 1.27 cm, x/L = 0.5)	28	25	138	200	7	67	100	4	54	85

12 and 13 percent for C_f and between 26 and 28 percent for δ^*. The error in boundary-layer properties decreases very rapidly with time after the 50-K step change in total temperature (figs. 18 to 25). At a stagnation pressure of 2 atm, the error in boundary-layer properties is reduced to half its original value between 21 and 37 sec (see table II), even though the total time to reach an adiabatic condition may vary from approximately 3 min to slightly greater than 10 min. As would be expected, as time increases beyond the point where the error is cut in half the rate at which the boundary layer approaches an adiabatic wall condition decreases sharply.

The solid airfoil (figs. 18 and 19) requires about 300 sec to reach an adiabatic condition at p_t = 2 atm, and about 190 sec at p_t = 6 and 9 atm. The time for the airfoil to reach a condition where the error is 1 percent at p_t = 2 atm is 142 sec and 175 sec for the C_f and δ^* error, respectively. The times required to reach the 1-percent error level are always less for the C_f error than for the δ^* error because the initial maximum error for C_f is about half that of δ^*. The times for the 1-percent error condition are somewhat less for the 6- and 9-atm condition as can be seen in table II.

The times to reach an adiabatic condition for the bodies of revolution (figs. 20 to 25) at p_t = 2 atm range from slightly greater than 600 sec for the solid body to 390 and 200 sec for the τ = 2.54 cm and τ = 1.27 cm hollow bodies, respectively. The solid body of revolution reaches an adiabatic condition in about 540 and 480 sec for p_t = 6 and 9 atm, respectively. The thicker-walled hollow body of revolution (τ = 2.54 cm) reaches an adiabatic condition in about 220 sec for p_t = 6 and 9 atm. The thinner-walled hollow body of revolution (τ = 1.27 cm) reaches an adiabatic condition in about 100 sec and 85 sec for p_t = 6 and 9 atm, respectively. The times to reach the condition where the

error in δ^* is 1 percent for p_t = 2 atm are 542, 298, and 138 sec for the solid, τ = 2.54 cm, and τ = 1.27 cm bodies of revolution, respectively. The times to reach the 1-percent error condition in C_f are somewhat less due to the lower initial maximum error as was noted for the airfoil (see table II). At the two higher pressures (6 and 9 atm) the times to reach the 1-percent error condition are significantly reduced as can be seen in table II.

CONCLUDING REMARKS

A theoretical analysis has been made of the time-varying effect of nonadiabatic wall conditions on two boundary-layer properties for a two-dimensional wing section and an axisymmetric fuselage section made from AISI type 310S stainless steel. The wing and fuselage sections are representative of the wing root chord and fuselage of a typical transport model for the National Transonic Facility. The analysis was made with a solid wing and three fuselage configurations (one solid and two hollow with skin thicknesses of 2.54 and 1.27 cm). The displacement thickness and local skin friction were investigated at a station on the model after a 50-K step change in total temperature in terms of the time required for these two boundary-layer properties to reach an adiabatic wall condition. The results of the time-varying analysis showed that if the axisymmetric body is made hollow with a moderately thin skin, its time constants are approximately those of the airfoil. For example, decreasing the wall thickness from 2.54 cm to 1.27 cm approximately cuts the time to reach an adiabatic condition in half. In general, the time to reach an adiabatic condition decreases significantly with an increase in stagnation pressure.

The nonlinearity of the cooling process after the 50-K step change results in a pronounced increase in time to reach an adiabatic condition over the time to reduce the maximum error by 50 percent. For instance, at a stagnation pressure of 2 atm (1 atm = 101.3 kPa) the error in boundary-layer properties is reduced to half its original value in between 21 and 37 sec, even though the total time to reach an adiabatic condition can be slightly in excess of 10 min.

The variation of the ratio of the local skin friction to the adiabatic wall value of local skin friction, as a function of the wall-to-total temperature ratio, was found to be nearly independent of the stagnation pressure from 2 to 9 atm and stagnation temperatures from room temperature to cryogenic conditions. In addition, the ratio of displacement thickness to the adiabatic wall value of skin friction was found to be nearly independent of stagnation temperature, from the room temperature to cryogenic conditions, but was dependent on the level of stagnation pressure.

Langley Research Center
National Aeronautics and Space Administration
Hampton, VA 23665
April 3, 1980

REFERENCES

1. Nicks, Oran W.; and McKinney, Linwood W.: Status and Operational Characteristics of the National Transonic Facility. AIAA Paper 78-770, Apr. 1978.

2. McKinney, Linwood W.; and Howell, Robert R.: The Characteristics of the Planned National Transonic Facility. Proceedings of 9th Aerodynamics Testing Conference, June 1976, pp. 176-184.

3. Howell, Robert R.; and McKinney, Linwood W.: The U.S. 2.5-Meter Cryogenic High Reynolds Number Tunnel. High Reynolds Number Research, Donald D. Baals, ed., NASA CP-2009, 1977, pp. 27-51.

4. Kilgore, Robert A.; Igoe, William B.; Adcock, Jerry B.; Hall, Robert M.; and Johnson, Charles B.: Full-Scale Aircraft Simulation With Cryogenic Tunnels and Status of the National Transonic Facility. NASA TM-80085, 1979.

5. Chudyk, D. W.: Transonic Wind Tunnel Tests of Several NASA Bodies of Revolution. NASA CR-112069, 1971.

6. Hall, Robert M.: An Analysis of Data Related to the Minimum Temperatures for Valid Testing in Cryogenic Wind Tunnels Using Nitrogen as the Test Gas. NASA TM X-73924, 1976.

7. Anderson, E. C.; and Lewis, C. H.: Laminar or Turbulent Boundary-Layer Flows of Perfect Gases or Reacting Gas Mixtures in Chemical Equilibrium. NASA CR-1893, 1971.

8. Haas, L. A.: Study of a Fail-Safe Abort System for an Actively Cooled Hypersonic Aircraft. NASA CR-144927, 1975.

9. Harris, Julius E.: Numerical Solution of the Equations for Compressible Laminar, Transitional, and Turbulent Boundary Layers and Comparisons With Experimental Data. NASA TR R-368, 1971.

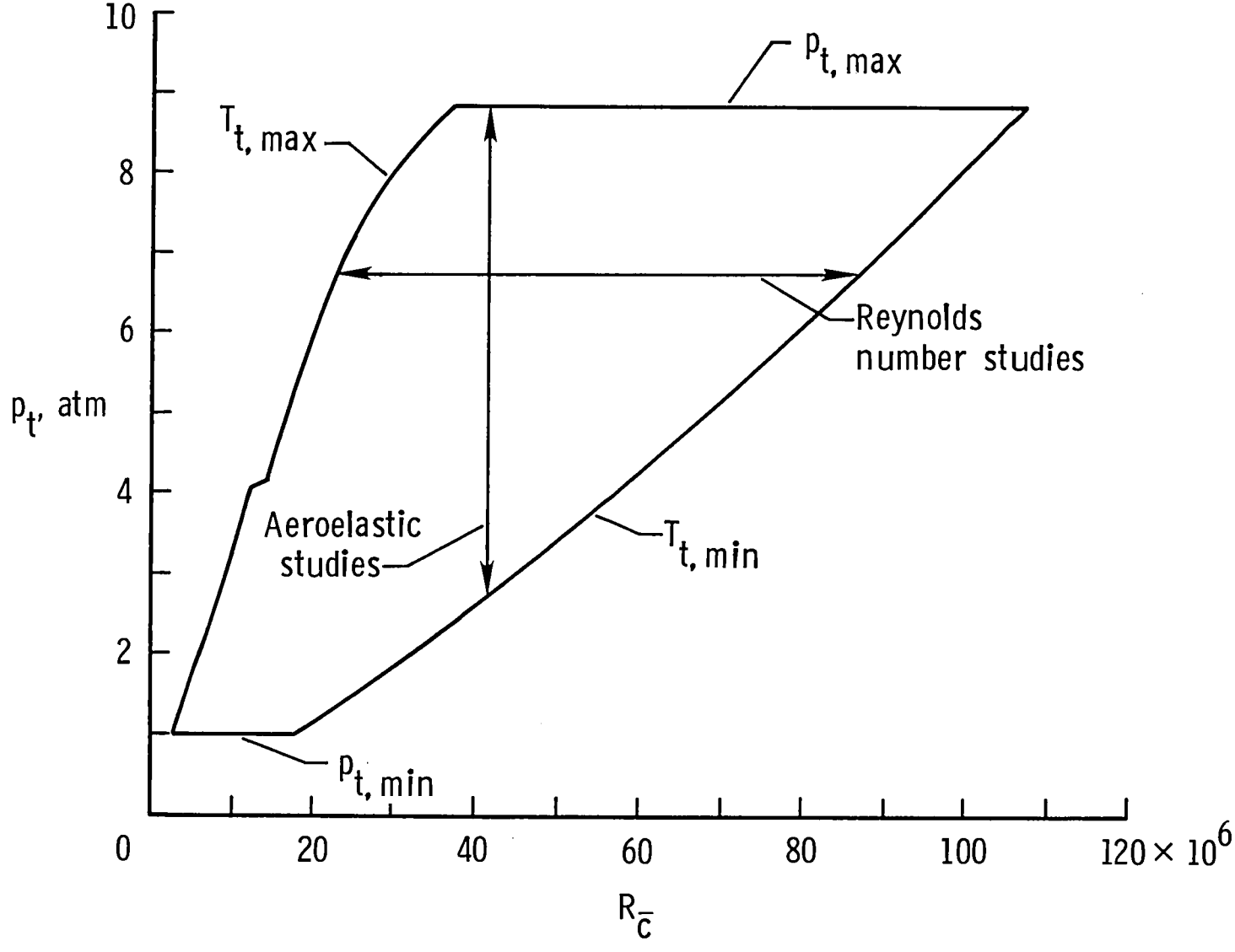

(a) Total pressure and total temperature limits.

Figure 1.- NTF operating envelope at $M_\infty = 0.80$. $\bar{c} = 0.25$ m.

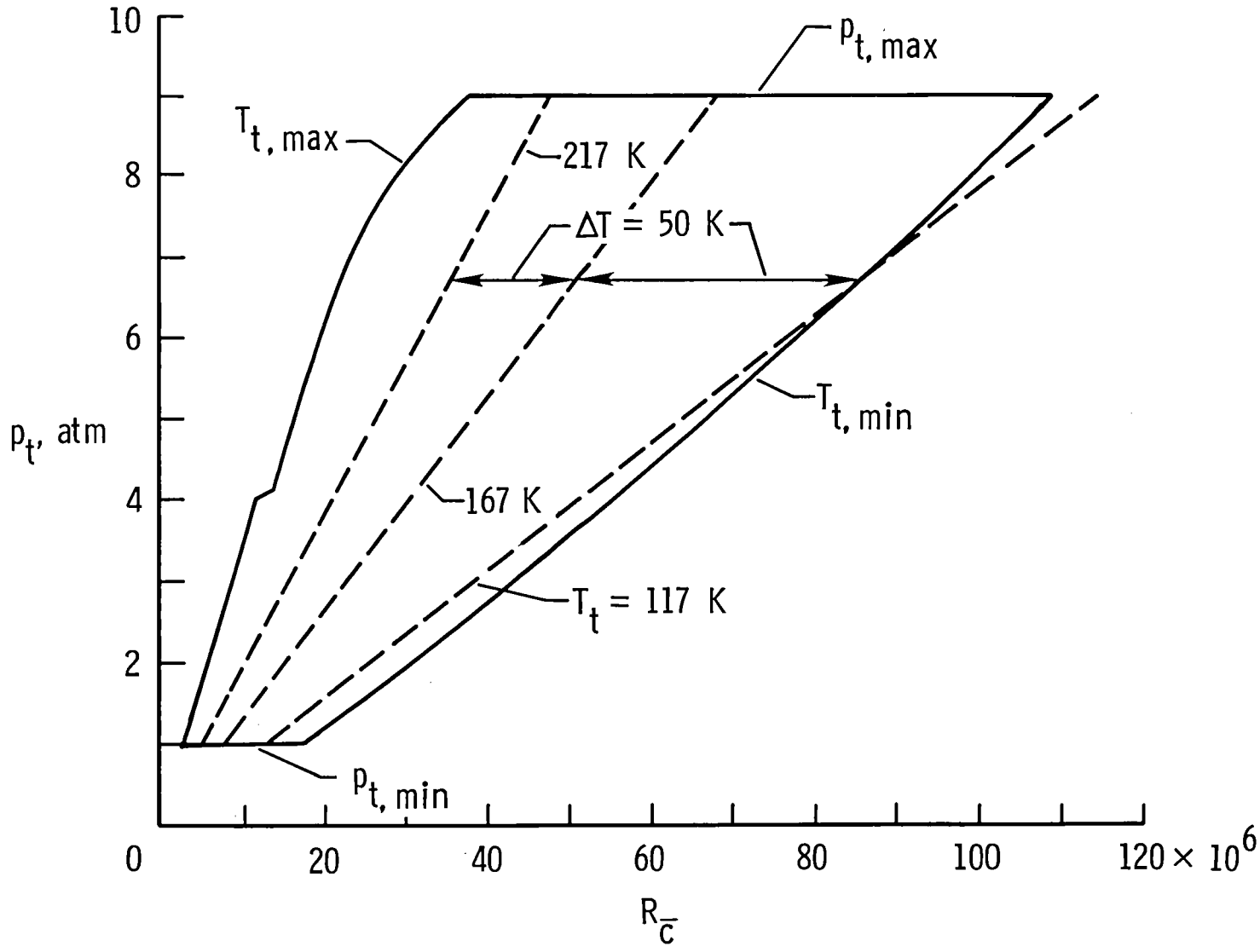

(b) Total temperature change in pure Reynolds number study.

Figure 1.- Concluded.

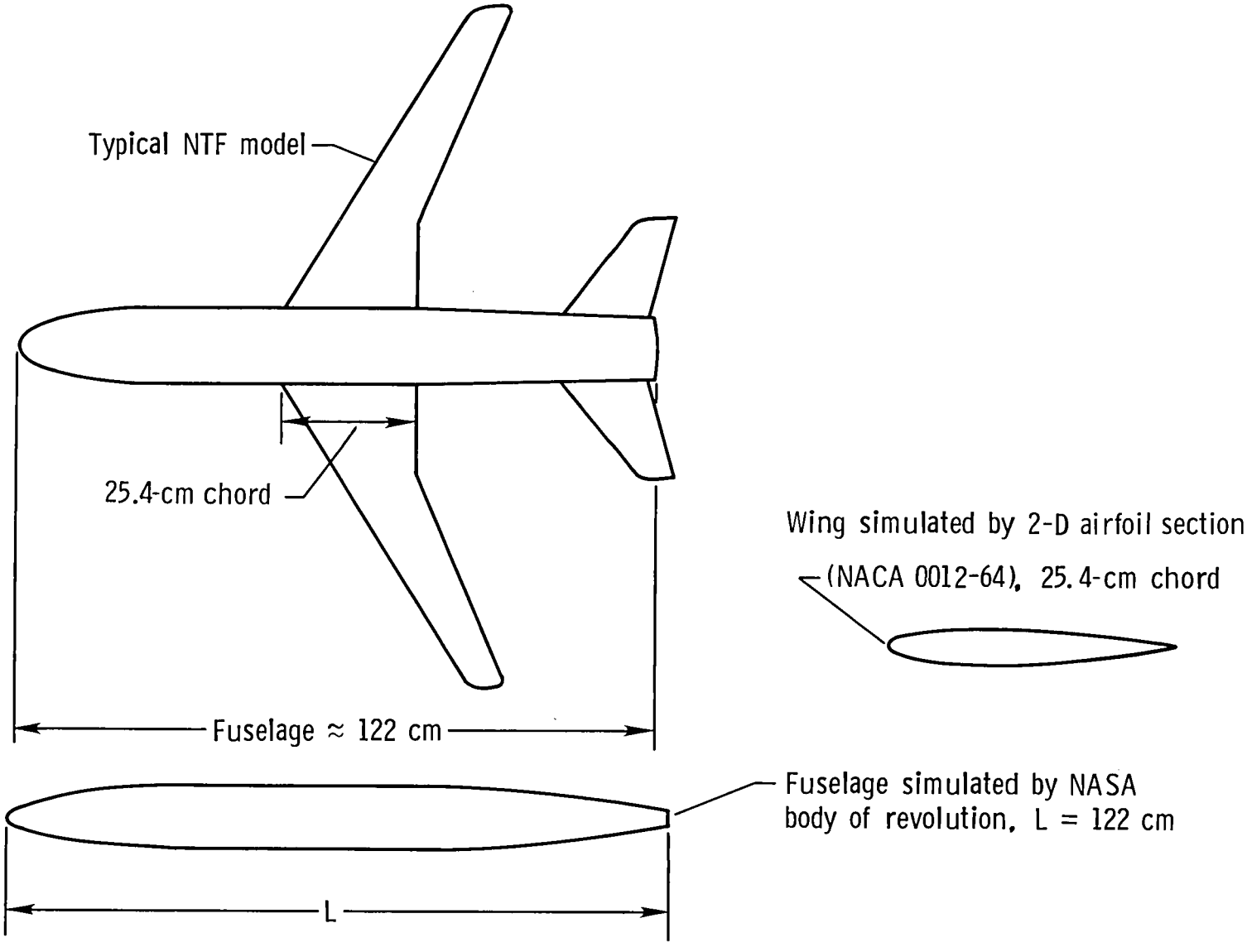

Figure 2.- Simulation of wing and fuselage sections for conduction analysis.

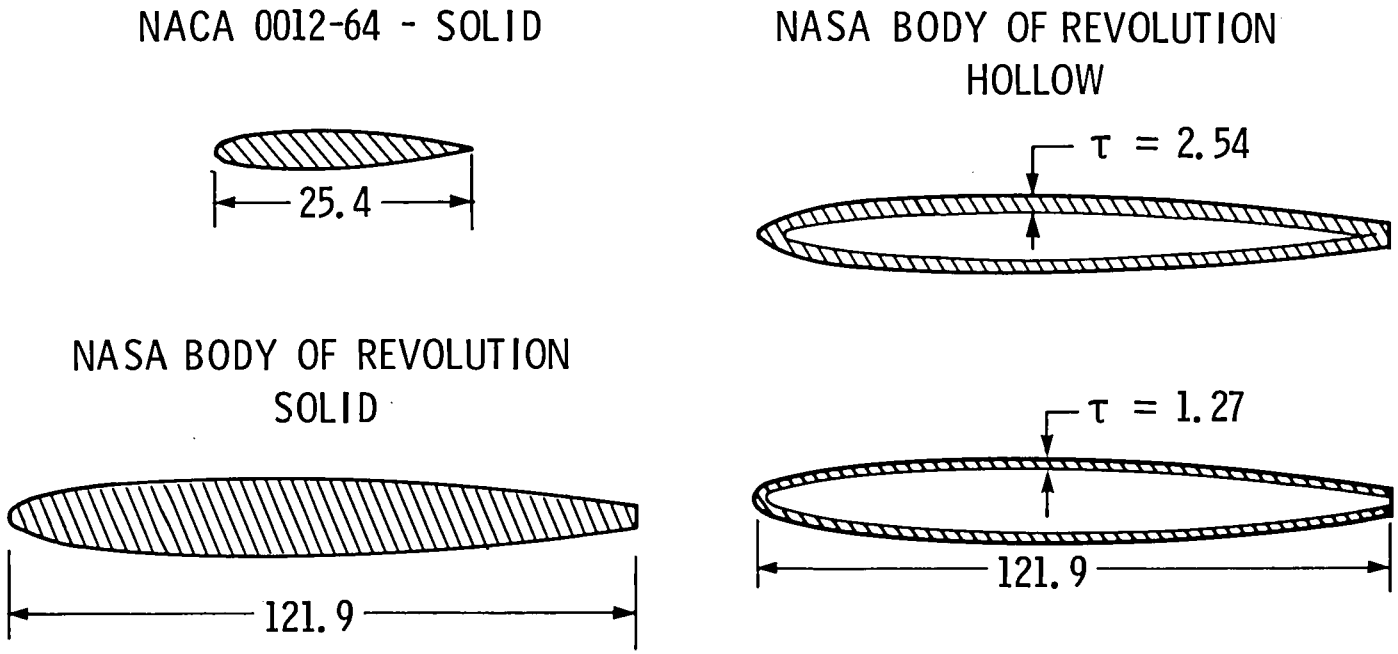

Figure 3.- One airfoil and three fuselage shapes tested for time to reach an adiabatic wall condition. All dimensions are in cm.

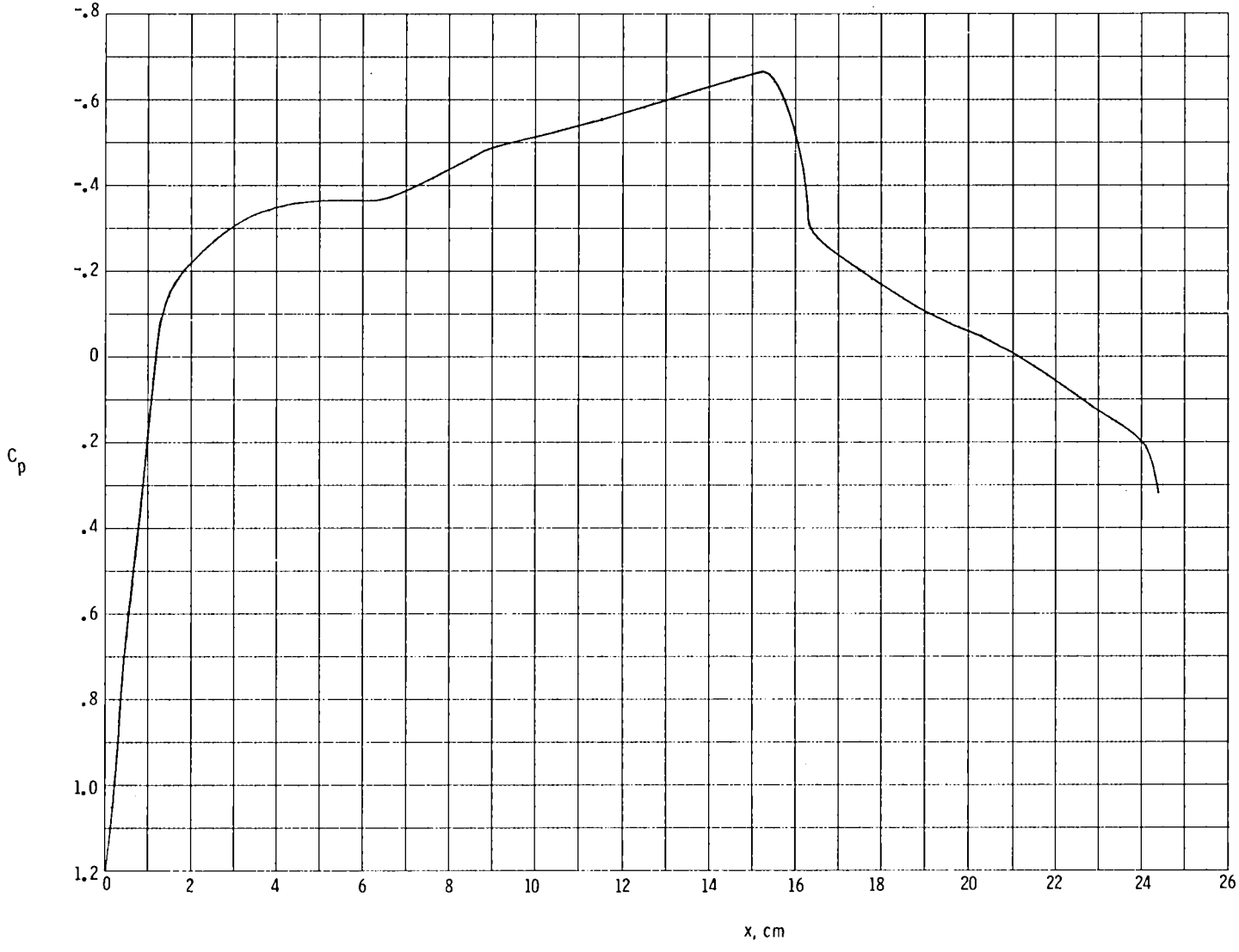

Figure 4.- Pressure distribution used for all boundary-layer calculations for the NACA 0012-64 airfoil (based on data from ref. 6). $\alpha = 0^{\circ}$; $M_{\infty} = 0.85$; $p_t = 2.12$ atm; $T_t = 161.1$ K.

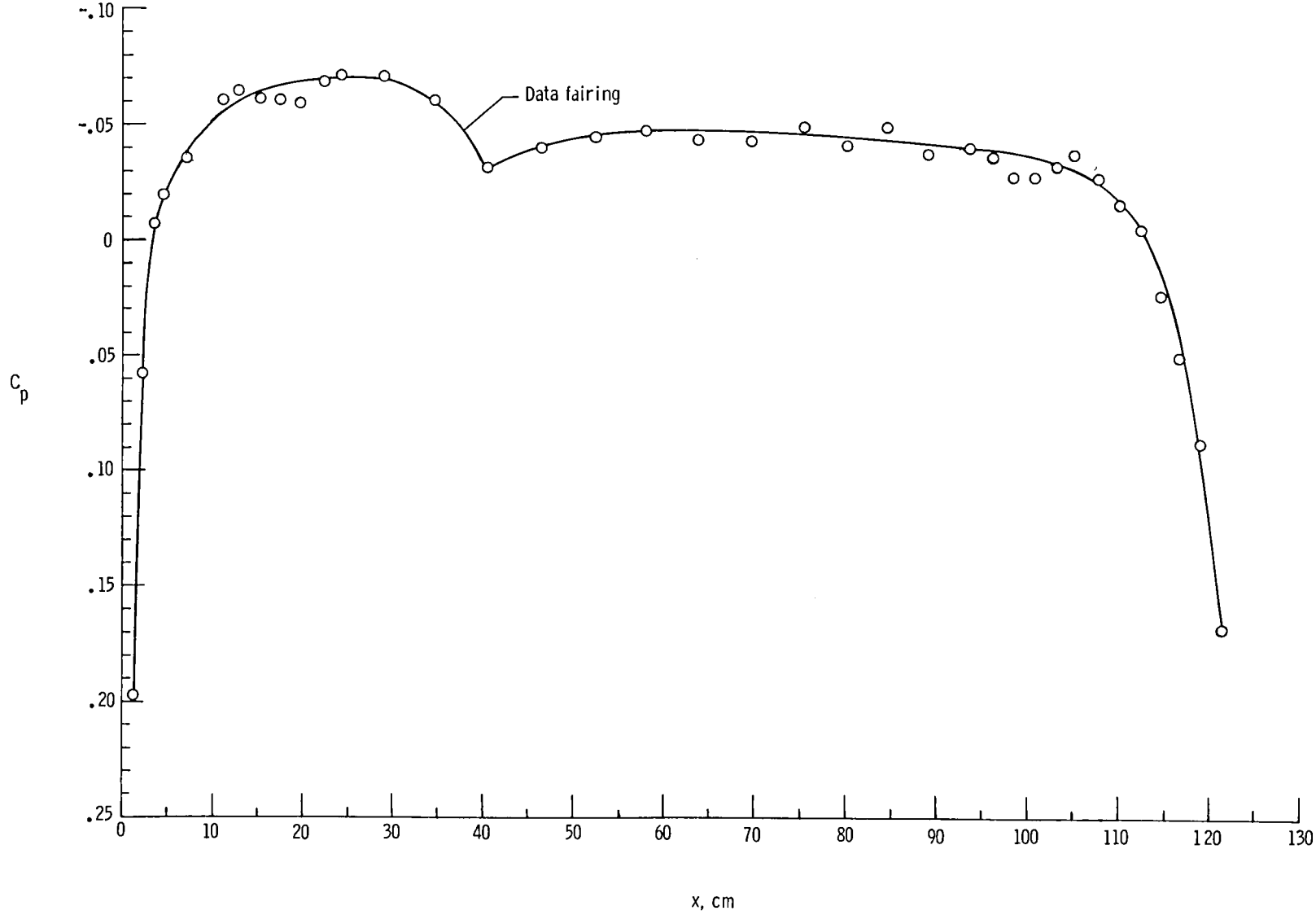

Figure 5.- Pressure distribution used for all boundary-layer calculations for the NASA body of revolution. $\alpha = 0^{\circ}$; $M_{\infty} = 0.852$; $L = 121.92$ cm; $p_t = 1$ atm; $T_t = 312$ K.

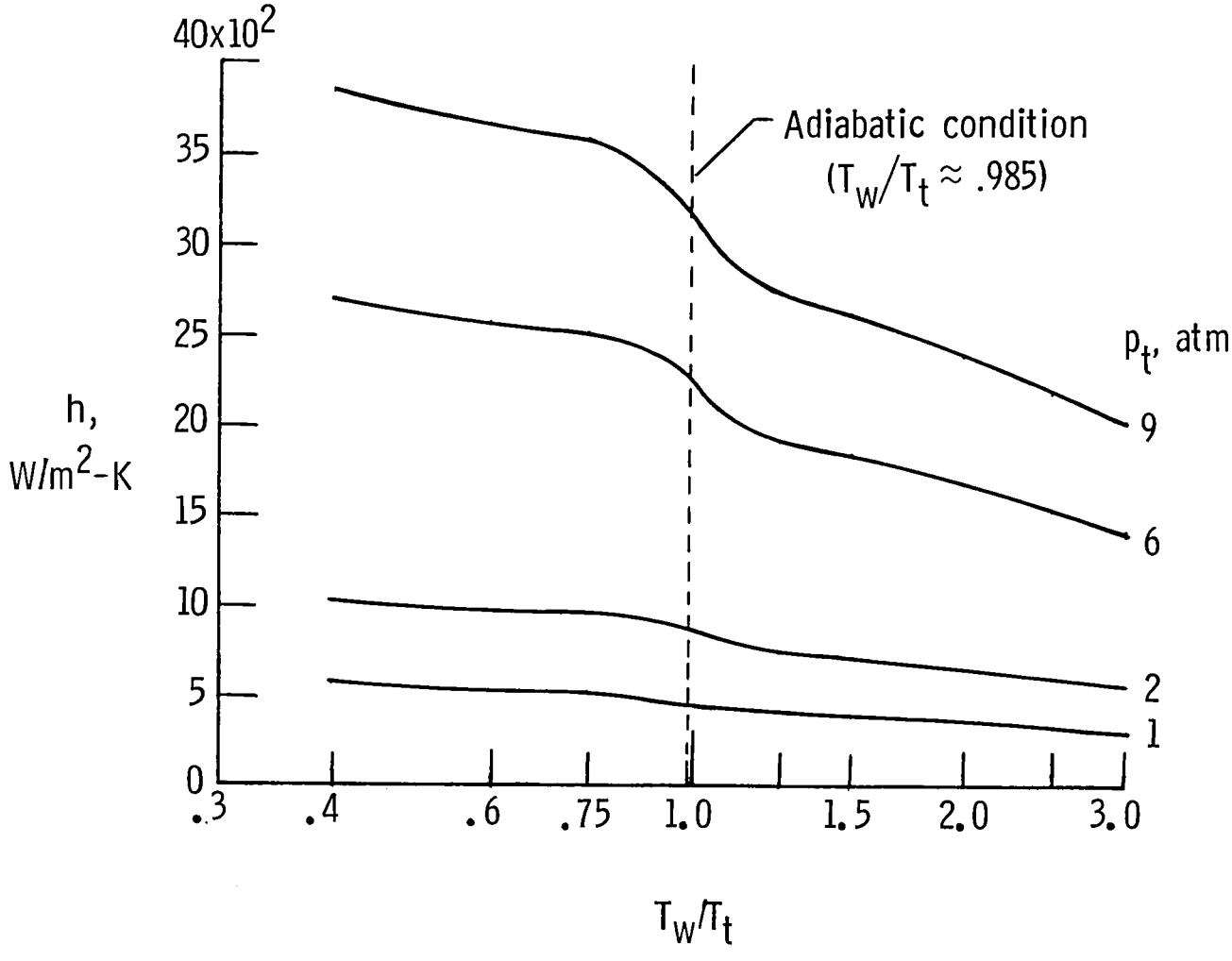

Figure 6.- The effect of the T_w/T_t ratio on h for various pressures on the NACA 0012-64 airfoil. x/c = 0.4; M_∞ = 0.85; c = 25.4 cm; T_t = 116 K; $\alpha = 0^o$.

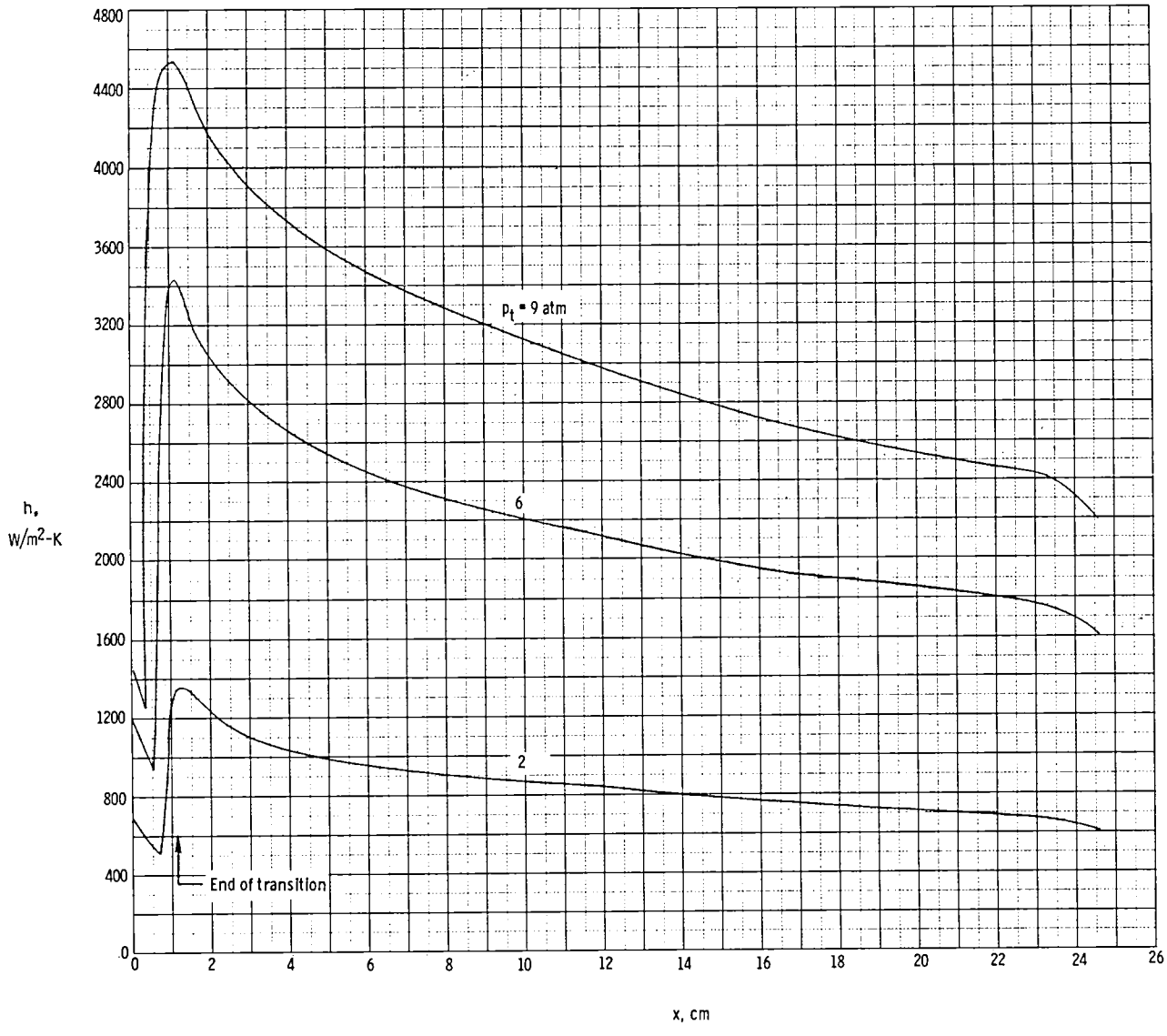

Figure 7.- The distribution of h used in the heat conduction analysis for the NACA 0012-64 airfoil at three stagnation pressures. $\alpha = 0^{\circ}$; $M_{\infty} = 0.85$; $T_t = 117$ K; $c = 25.4$ cm; $T_w/T_t = 1.22$.

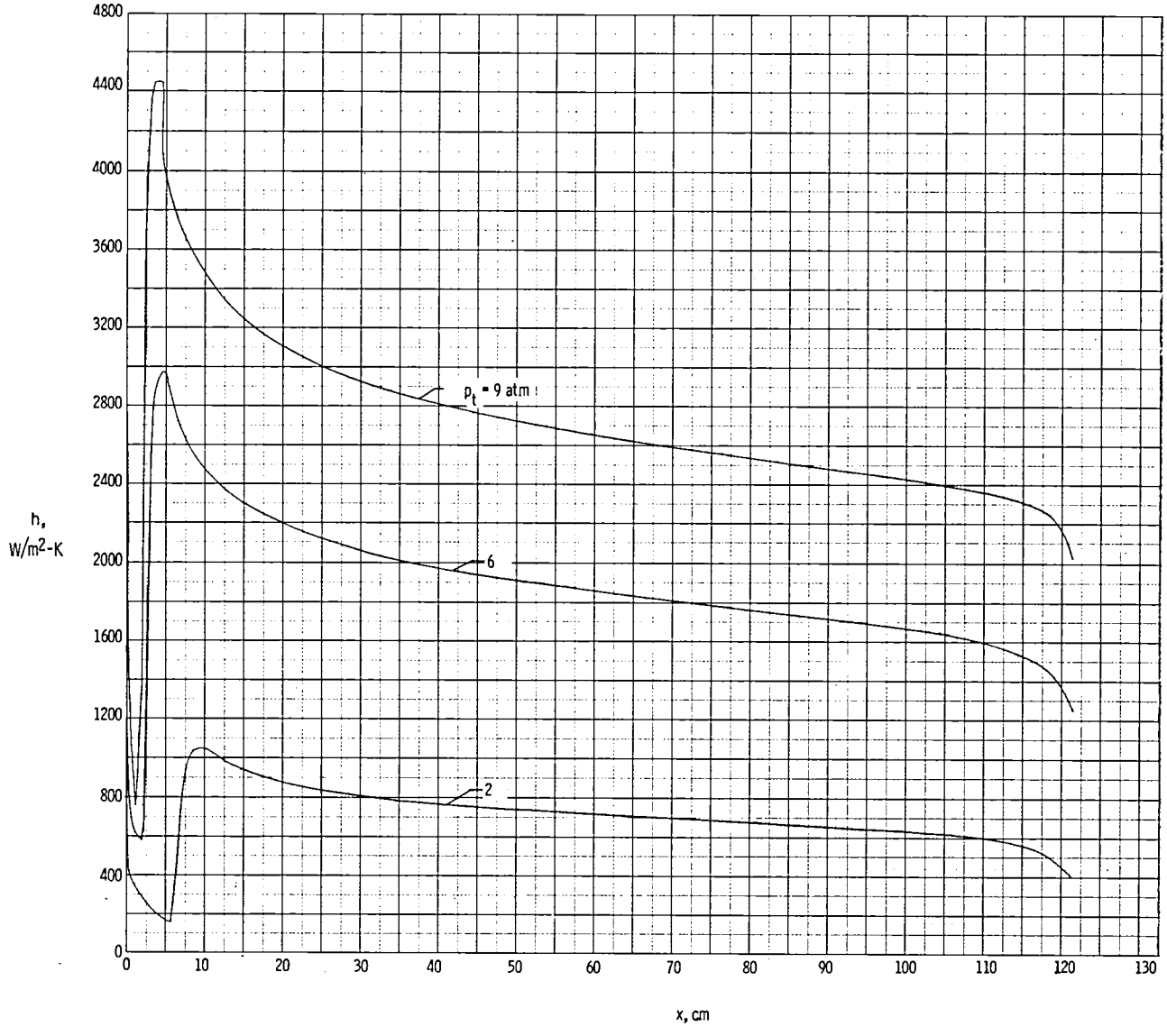

Figure 8.- The distribution of h used in the heat conduction analysis for the NASA body of revolution at three stagnation pressures. $\alpha = 0^{\circ}$; $M_{\infty} = 0.85$; $T_t = 117$ K; $L = 121.92$ cm; $T_w/T_t = 1.22$.

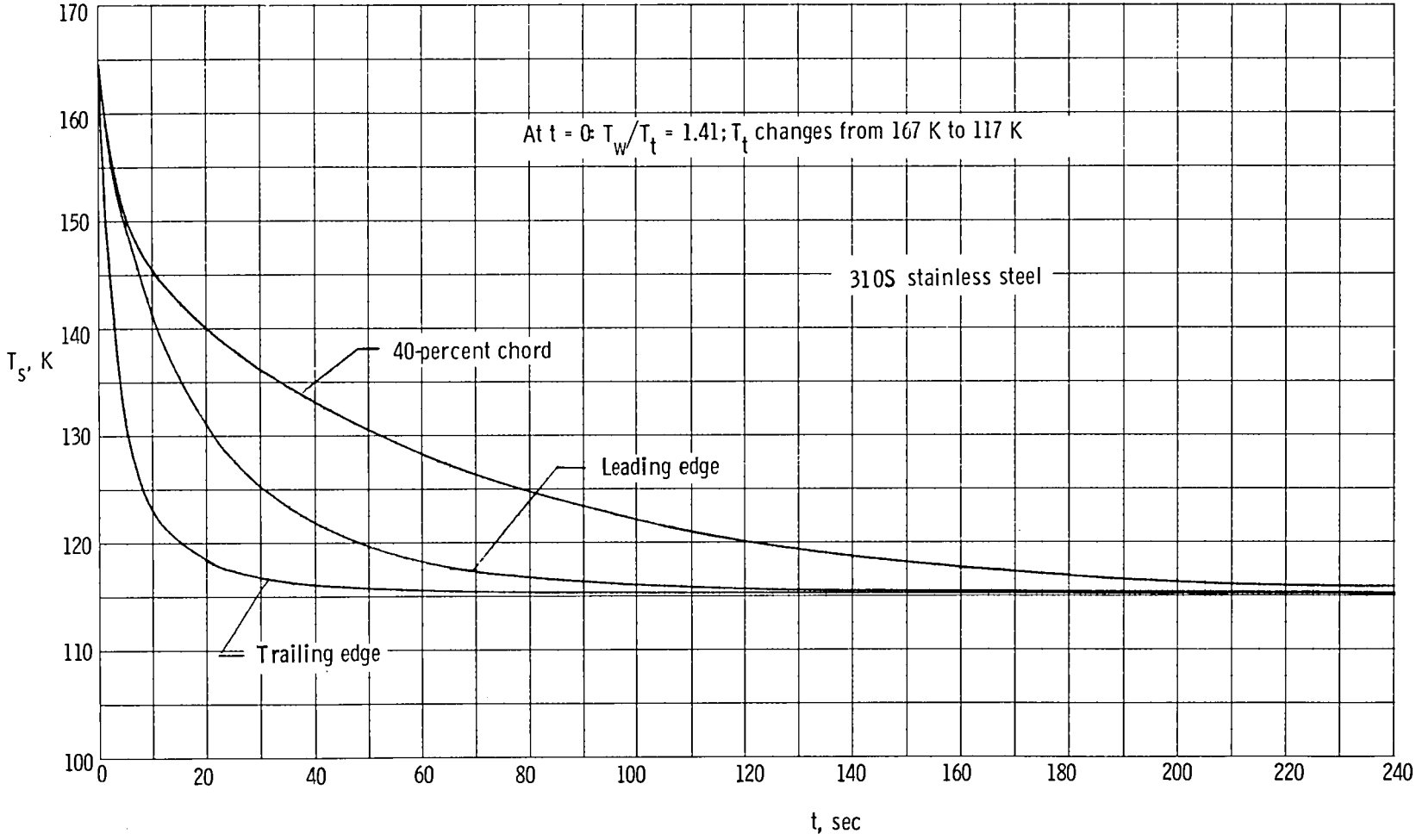

Figure 9.- The variation of surface temperature with time for three locations on the NACA 0012-64 airfoil for a 50-K step change in total temperature. M_∞ = 0.85; p_t = 2 atm; T_{aw} = 115.2 K; $\alpha = 0^\circ$; c = 25.4 cm; T_i = 164.5 K.

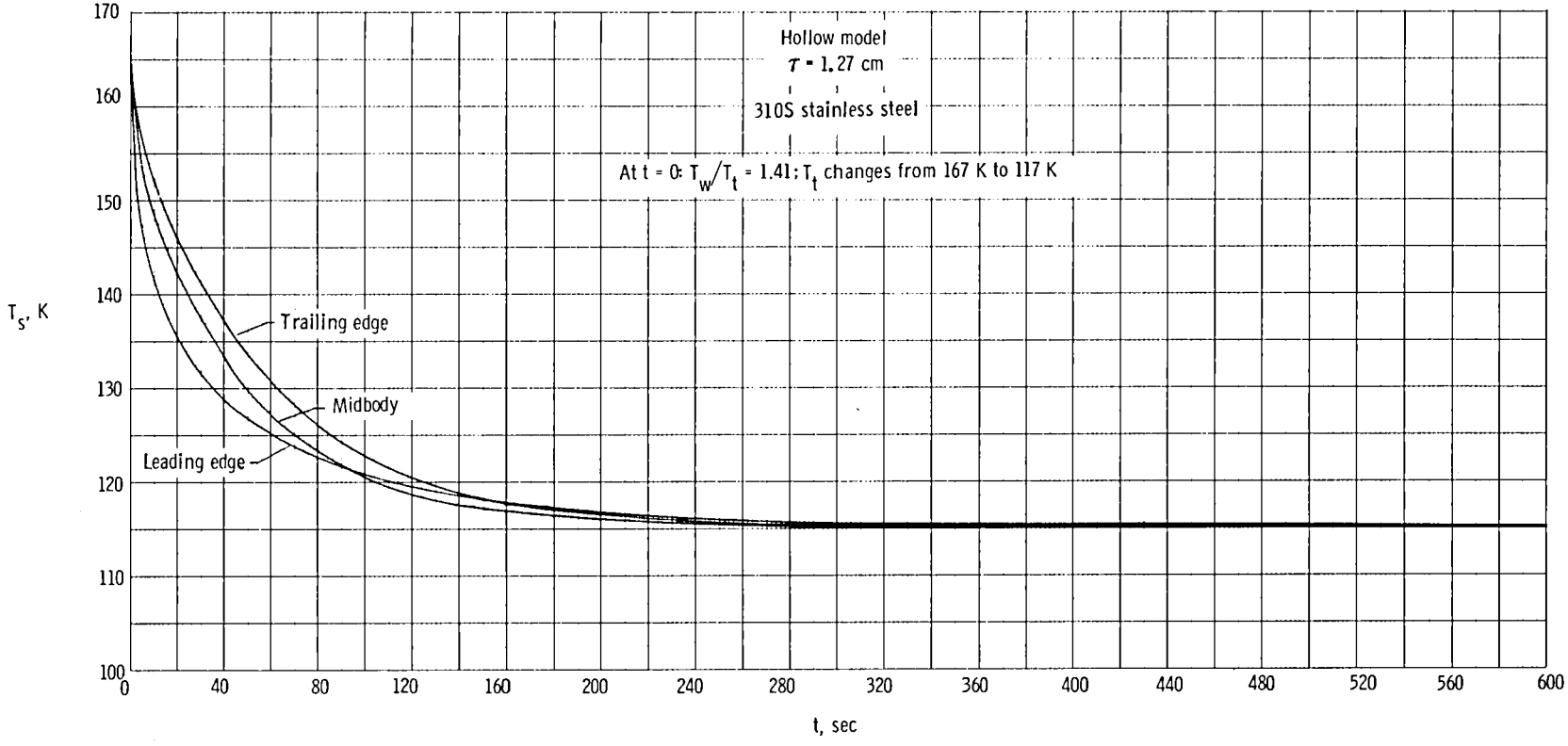

Figure 10.- The variation of surface temperature with time for three locations on the NASA body of revolution for a 50-K step change in total temperature. M_∞ = 0.85; p_t = 2 atm; T_{aw} = 115.2 K; α = 0°; L = 121.9 cm; T_i = 164.5 K.

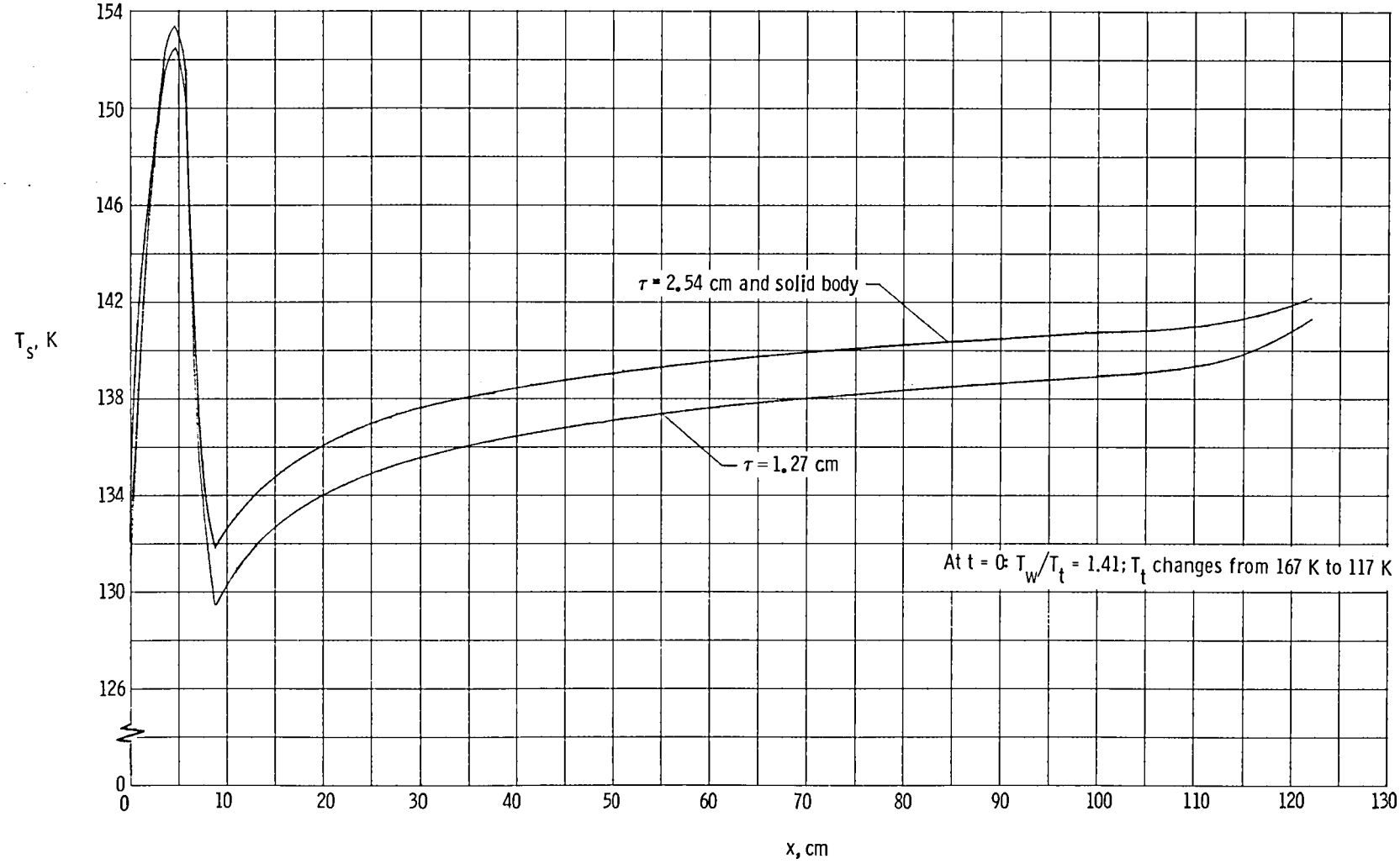

Figure 11.- The distribution of surface temperature for the three bodies of revolution 30 seconds after a 50-K step change in total temperature. L = 121.9 cm; M_∞ = 0.85; p_t = 2 atm; T_{aw} = 115 K.

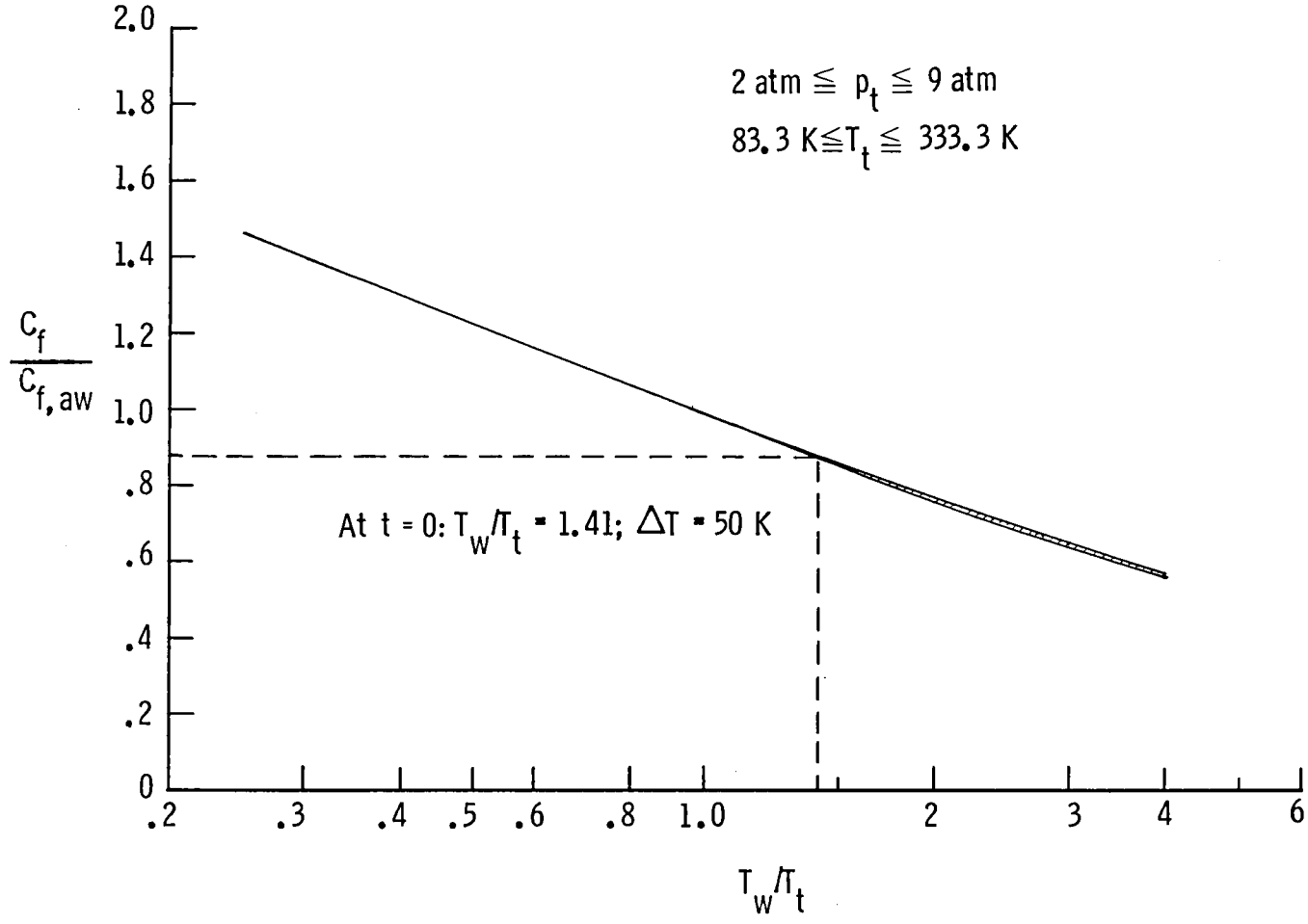

Figure 12.- The variation of C_f with the T_w/T_t ratio over a range of stagnation conditions for the NACA 0012-64 airfoil at x/c = 0.4. c = 25.4 cm; M_∞ = 0.85.

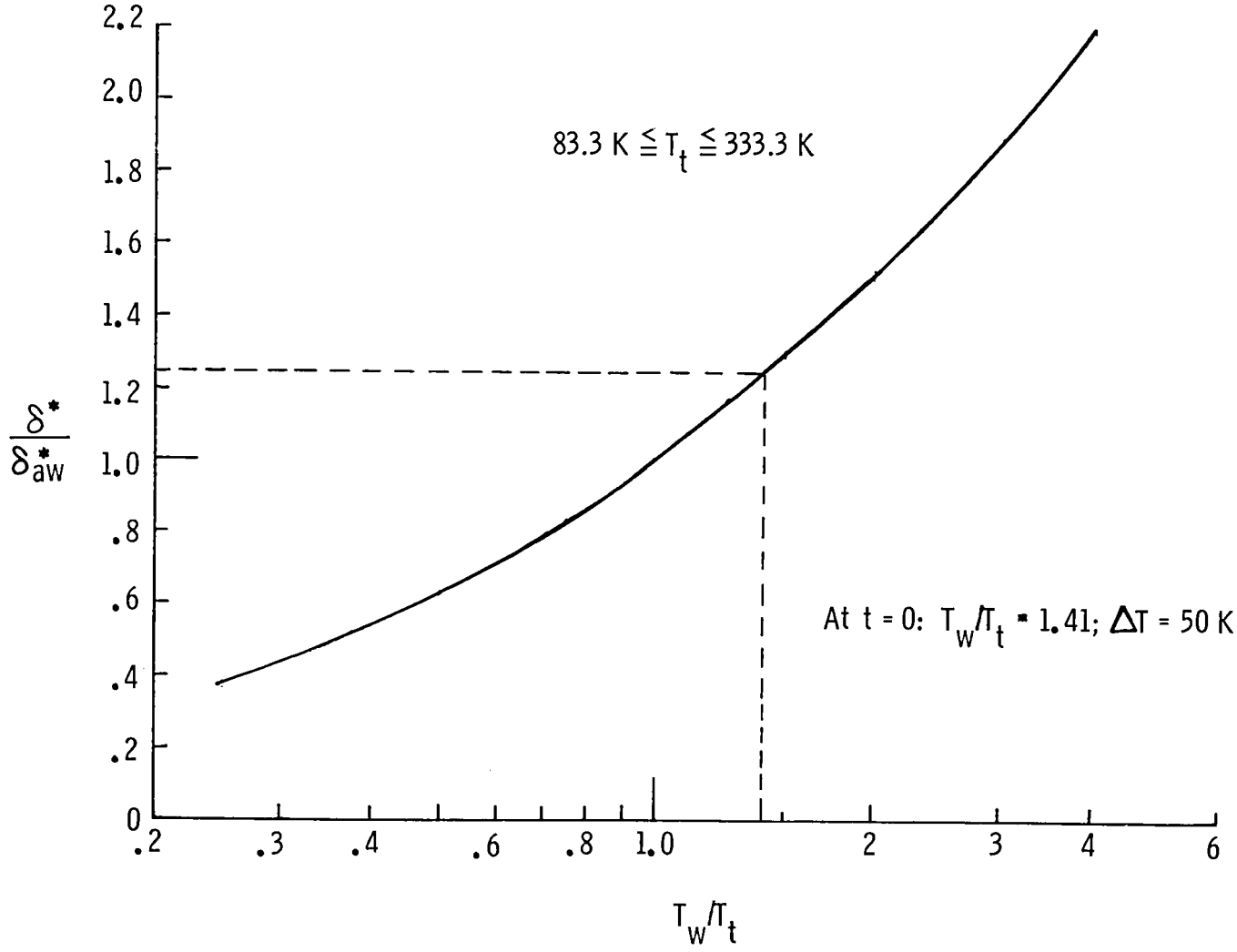

(a) p_t = 2 atm.

Figure 13.- The variation of δ^* with the T_w/T_t ratio over a range of stagnation conditions for the NACA 0012-64 airfoil at x/c = 0.4. c = 25.4 cm; M_∞ = 0.85.

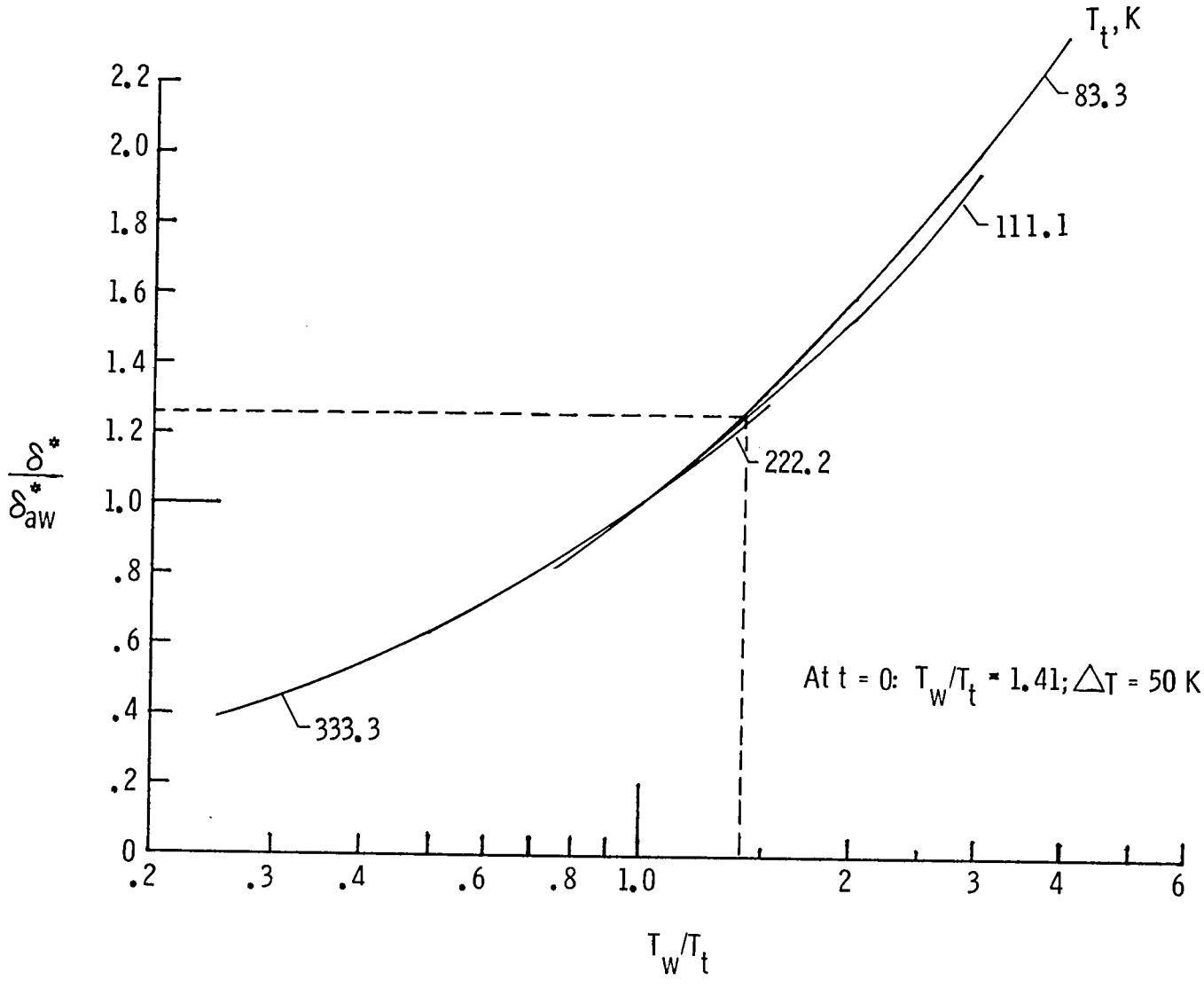

(b) p_t = 6 atm.

Figure 13.- Continued.

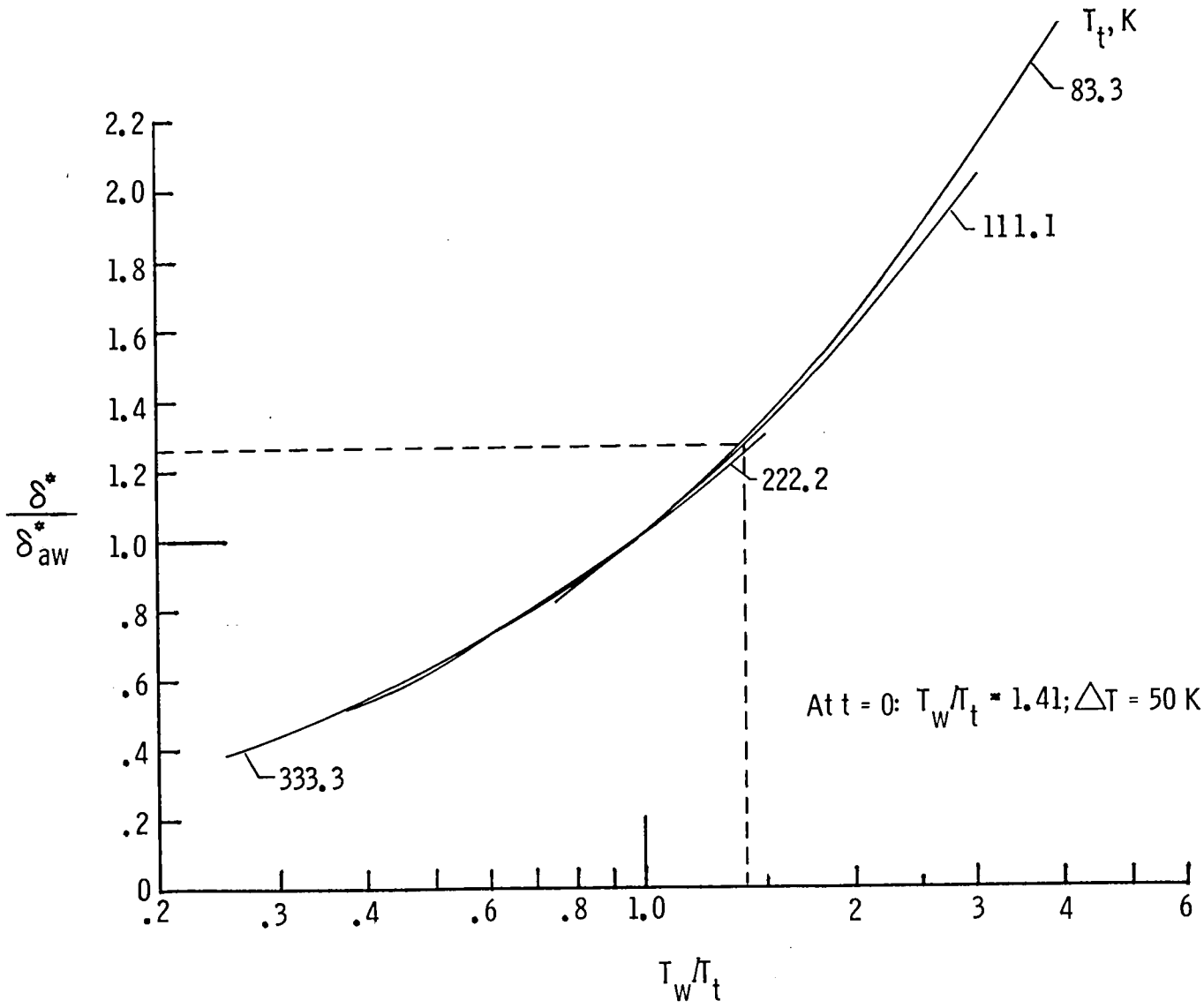

(c) p_t = 9 atm.

Figure 13.- Concluded.

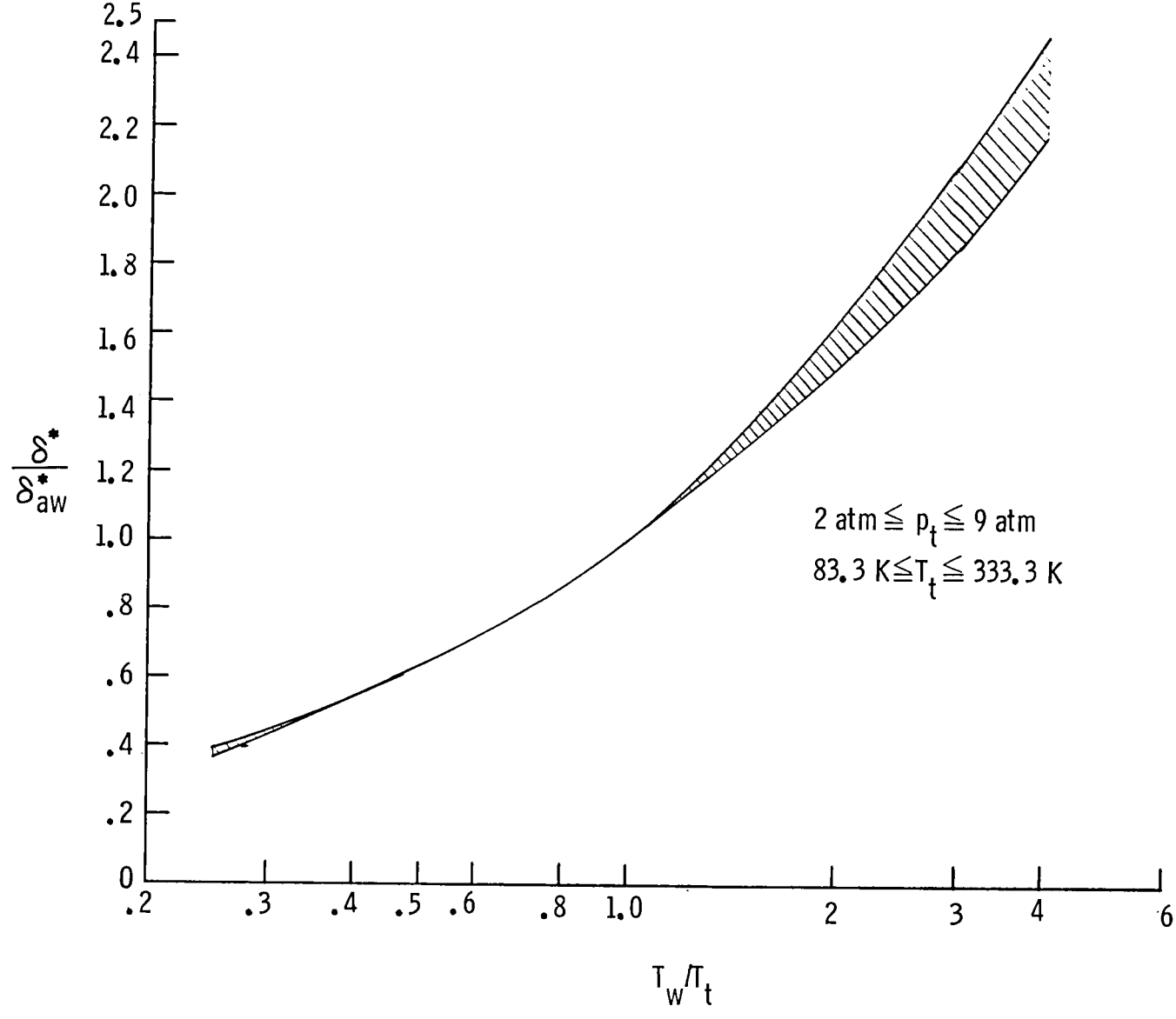

Figure 14.- The variation of δ^* with the T_w/T_t ratio over a range of stagnation conditions for the NACA 0012-64 airfoil at x/c = 0.4. c = 25.4 cm; M_∞ = 0.85.

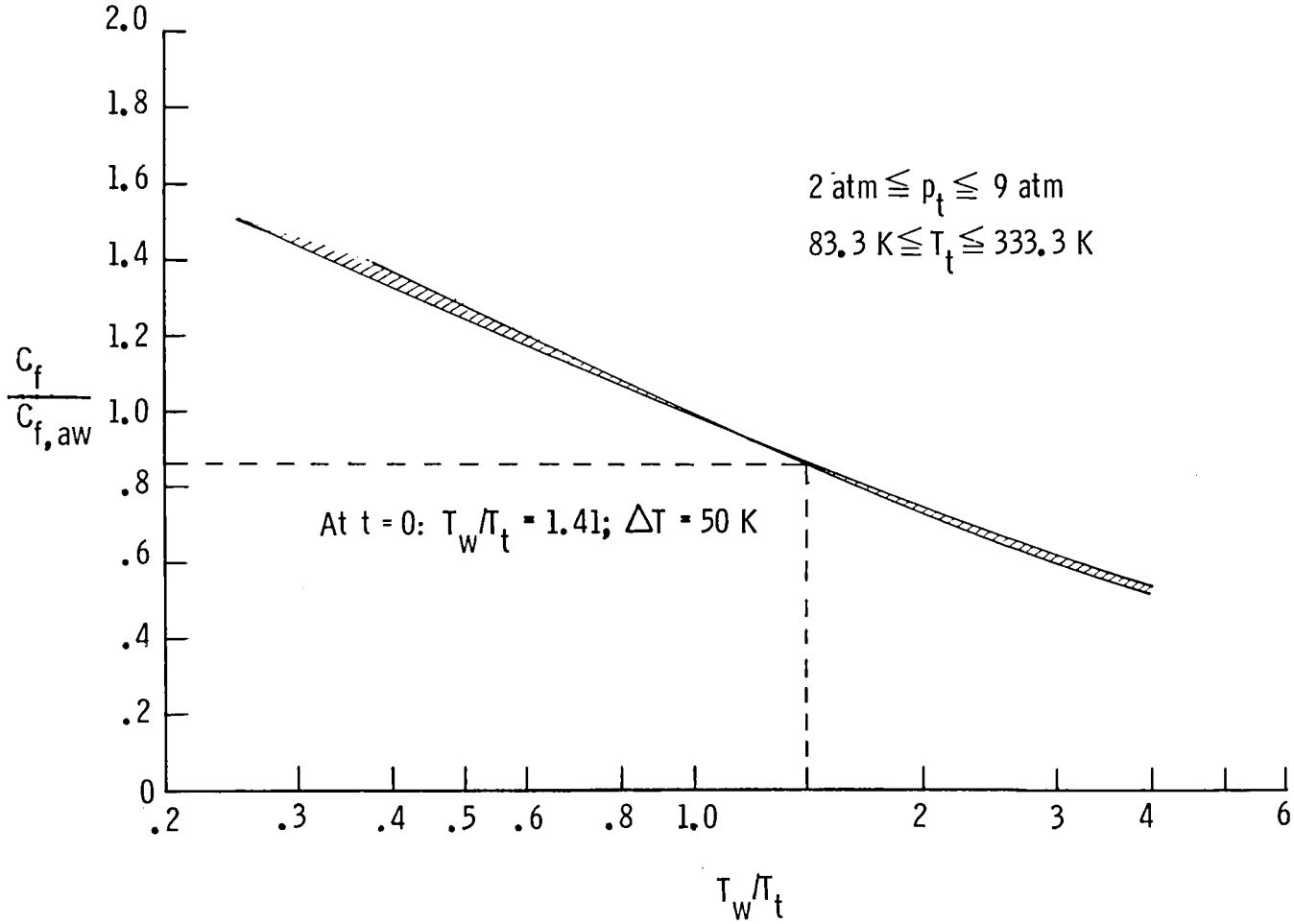

Figure 15.- The variation of C_f with the T_w/T_t ratio over a range of stagnation conditions for the NASA body of revolution at x/L = 0.50. L = 121.92 cm; M_∞ = 0.85.

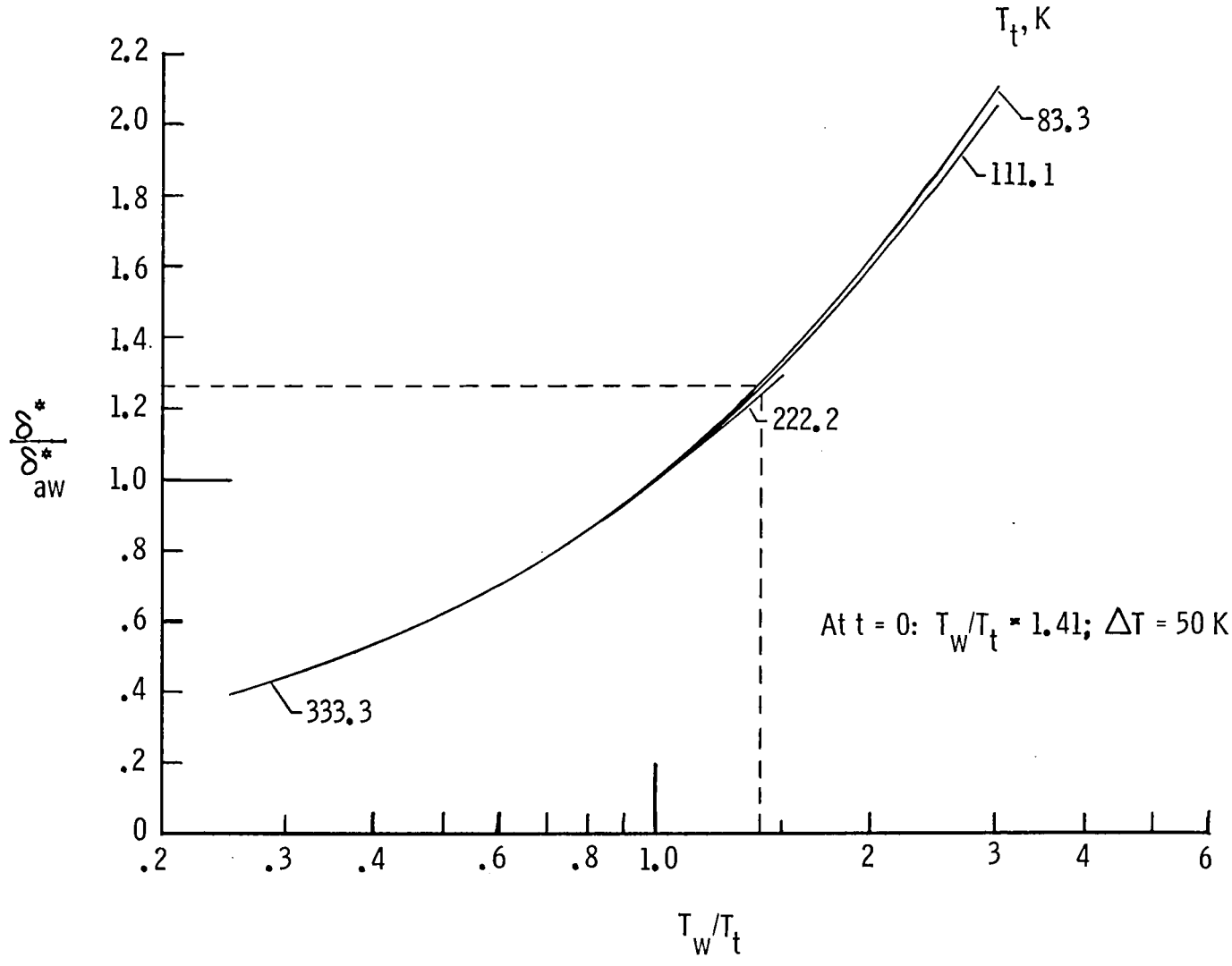

(a) p_t = 2 atm.

Figure 16.- The variation of δ^* with the T_w/T_t ratio over a range of stagnation conditions for the NASA body of revolution at x/L = 0.5. L = 121.92 cm; M_∞ = 0.85.

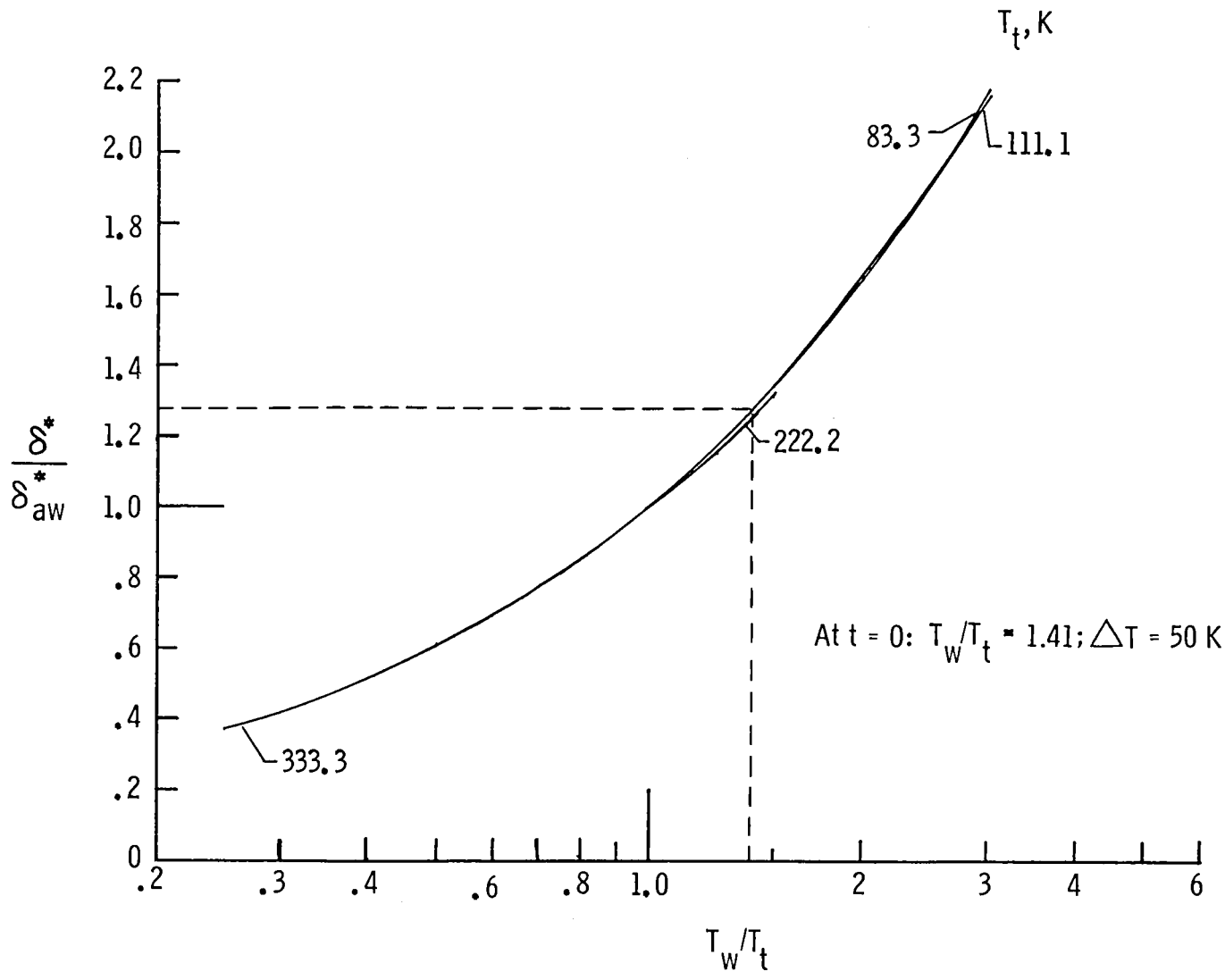

(b) p_t = 6 atm.

Figure 16.- Continued.

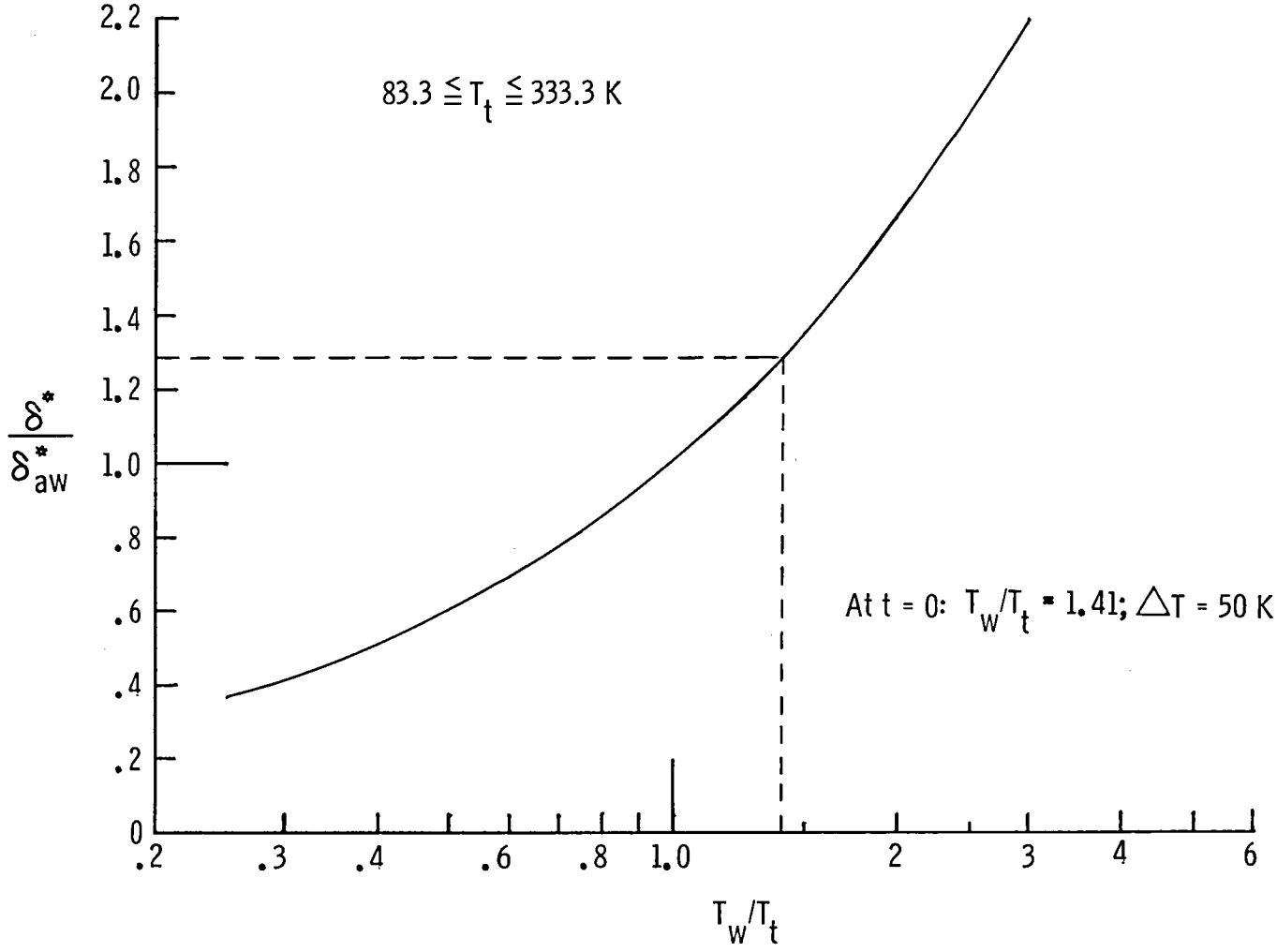

(c) p_t = 9 atm.

Figure 16.- Concluded.

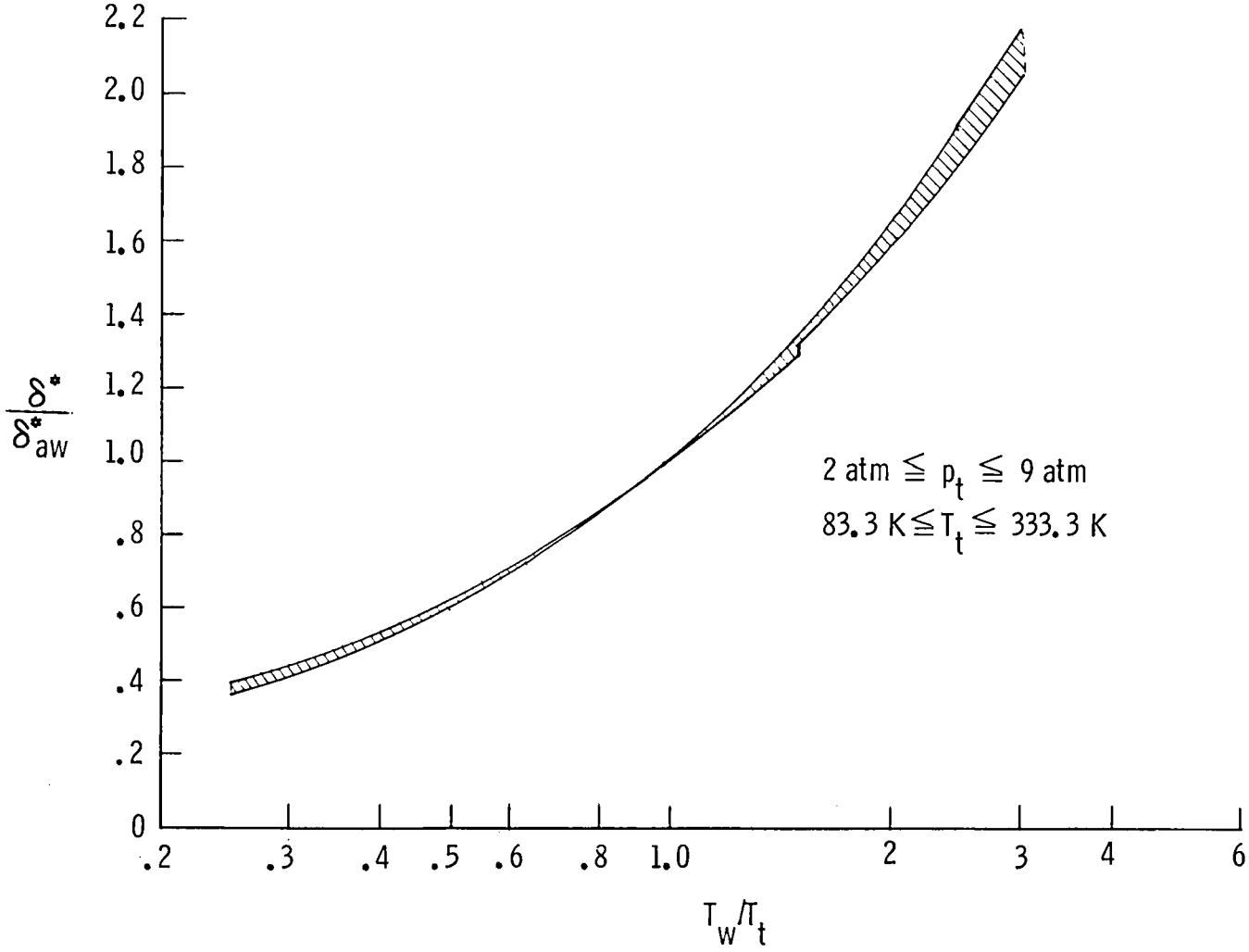

Figure 17.- The variation of δ^* with the T_w/T_t ratio over a range of stagnation conditions for the NASA body of revolution at x/L = 0.50. L = 121.92 cm; M_∞ = 0.85.

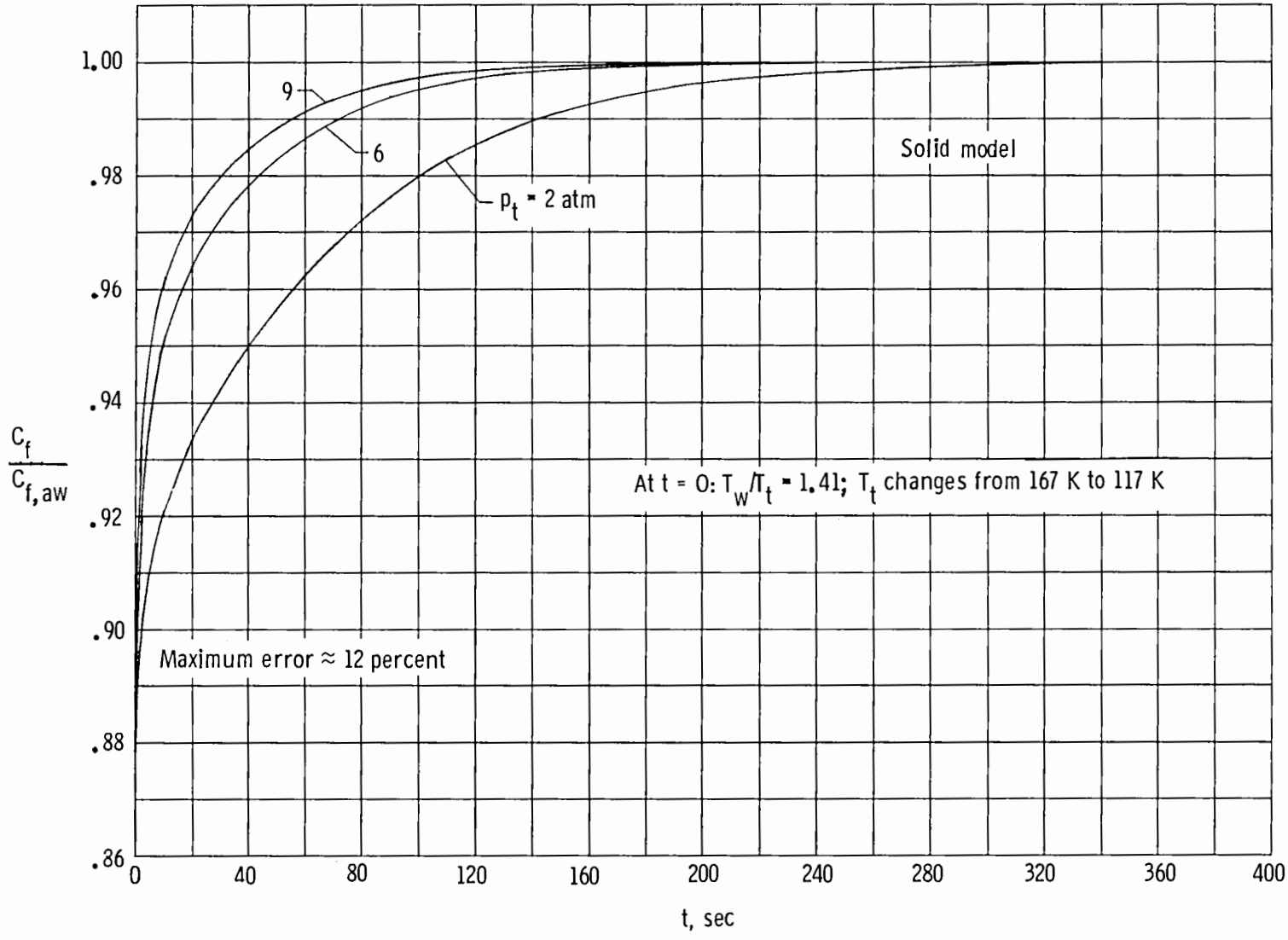

Figure 18.- Departure of C_f from $C_{f,aw}$ as a function of t for the NACA 0012-64 airfoil at x/c = 0.4. c = 25.4 cm; M_∞ = 0.85.

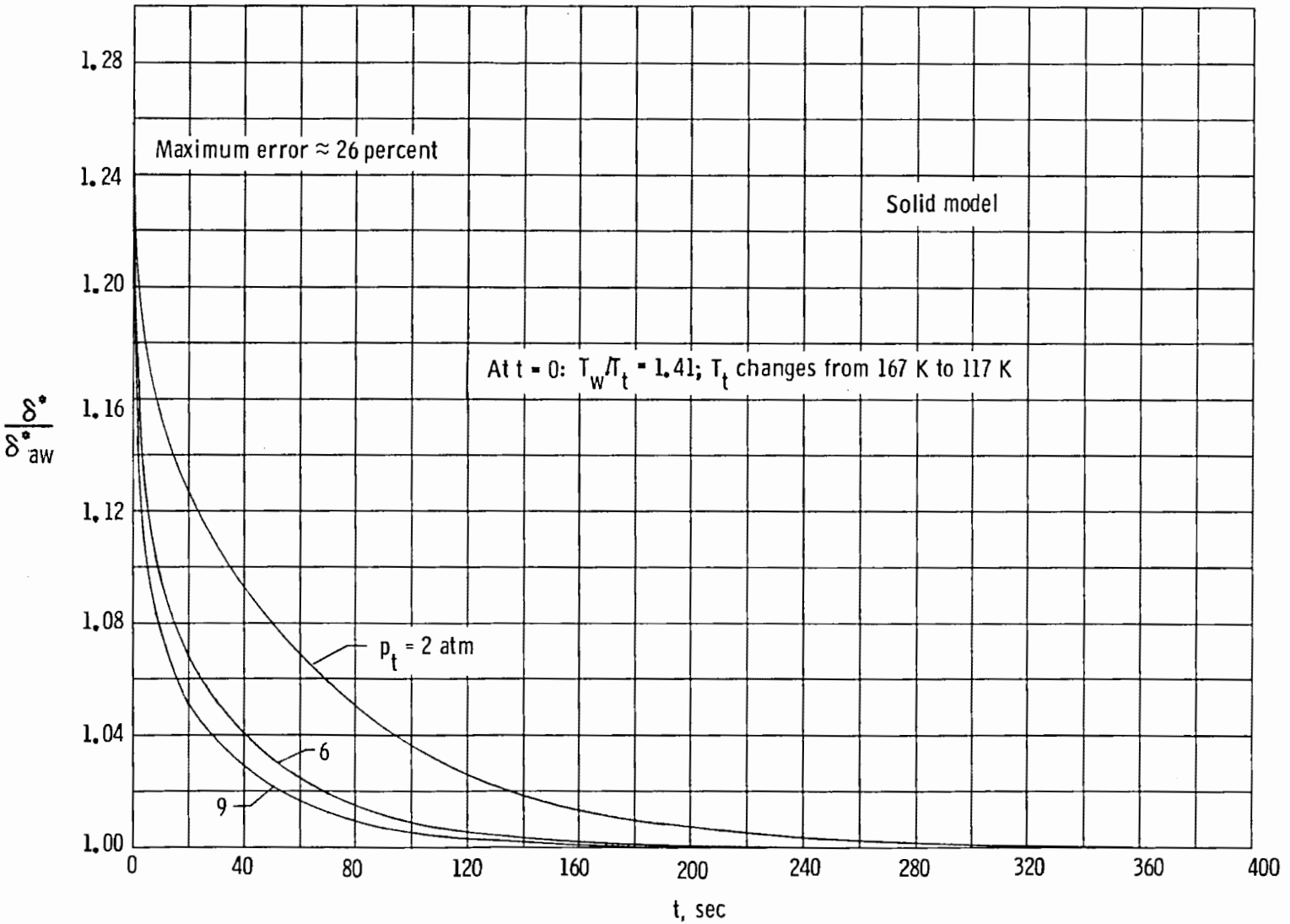

Figure 19.- Departure of δ^* from δ^*_{aw} as a function of t for the NACA 0012-64 airfoil at x/c = 0.4. c = 25.4 cm; M_∞ = 0.85.

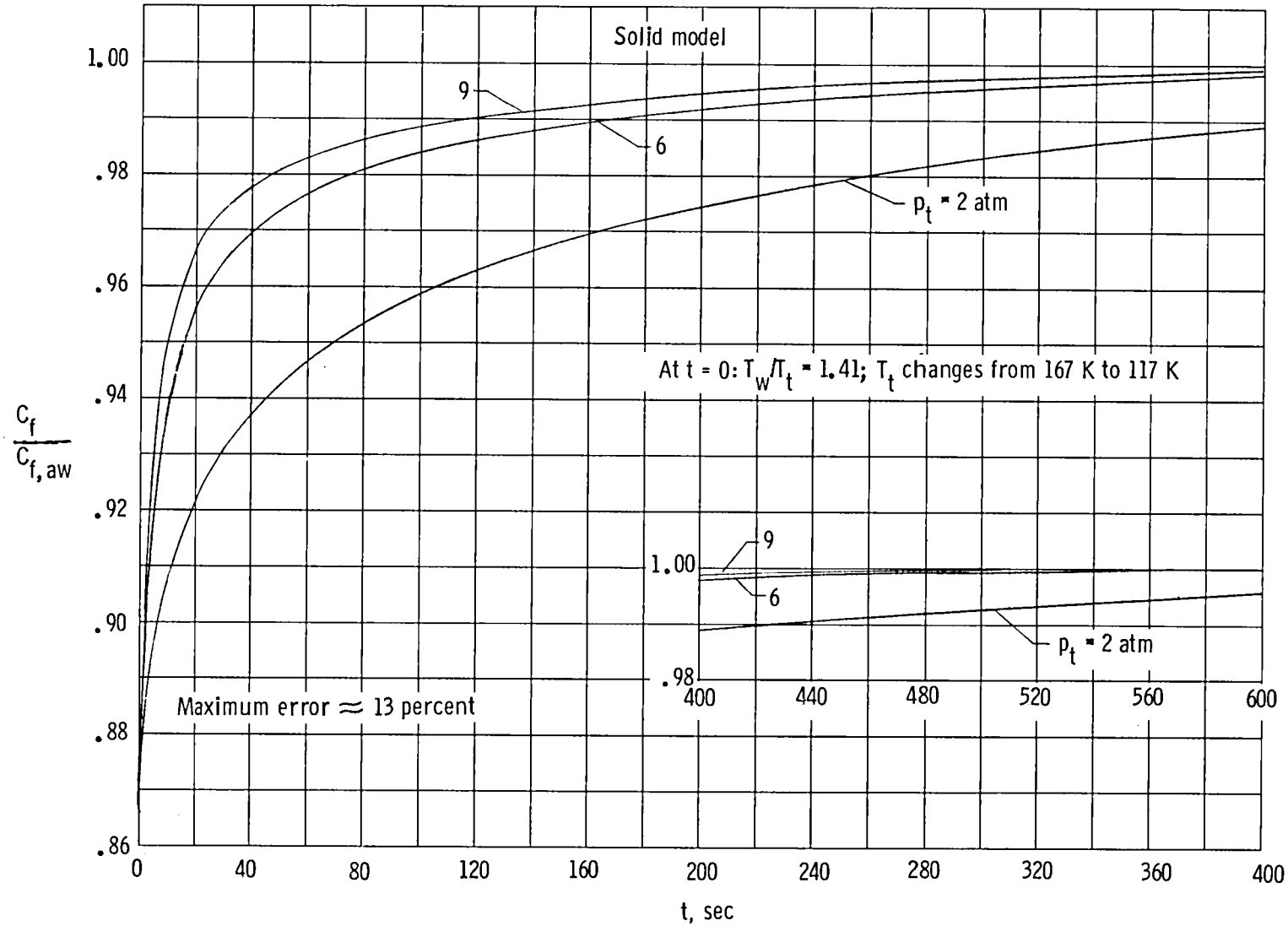

Figure 20.- Departure of C_f from $C_{f,aw}$ as a function of t for the NASA body of revolution at x/L = 0.5. L = 121.92 cm; M_∞ = 0.85.

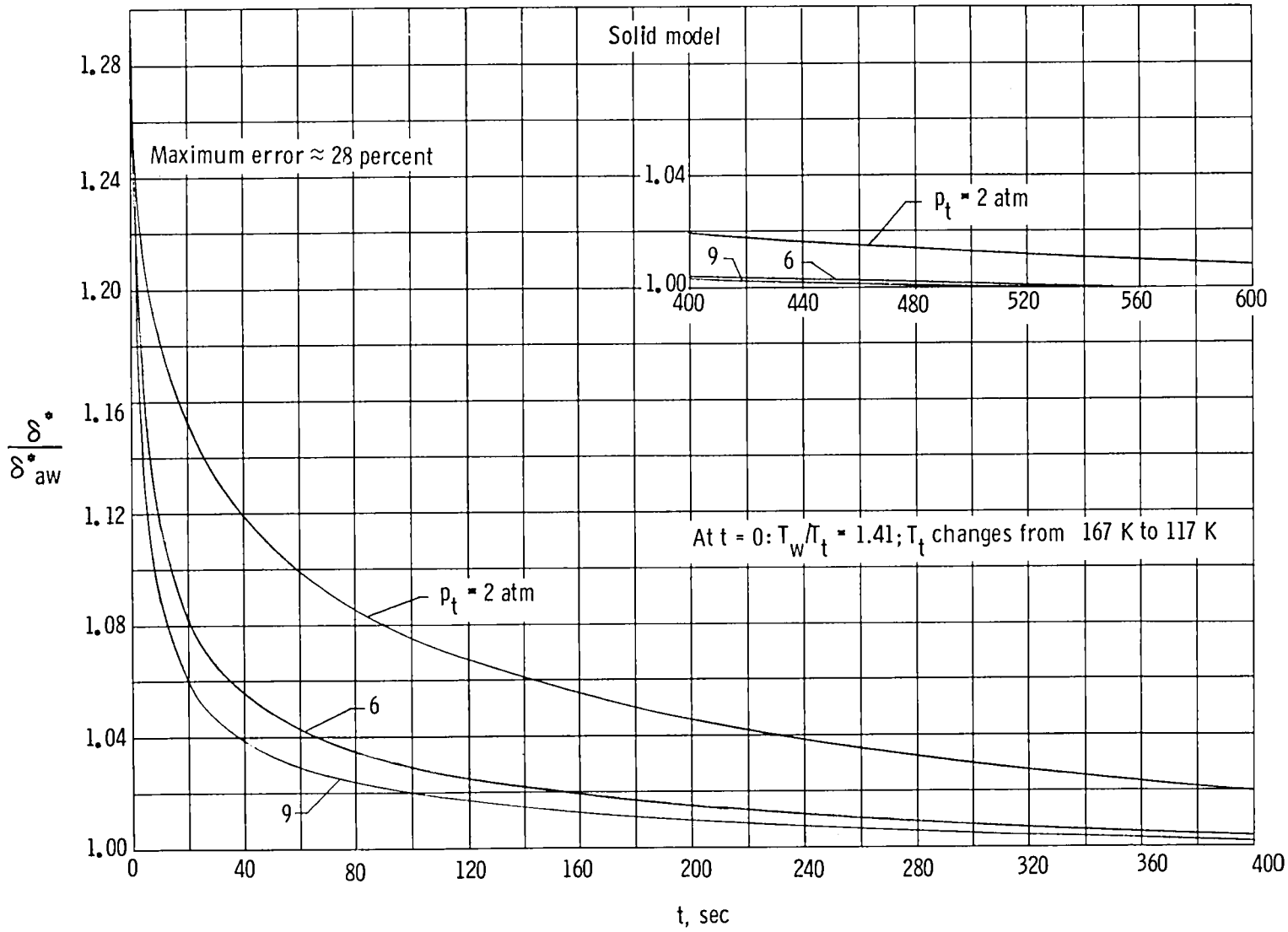

Figure 21.- Departure of δ^* from δ^*_{aw} as a function of t for the NASA body of revolution at x/L = 0.5. L = 121.92 cm; M_∞ = 0.85.

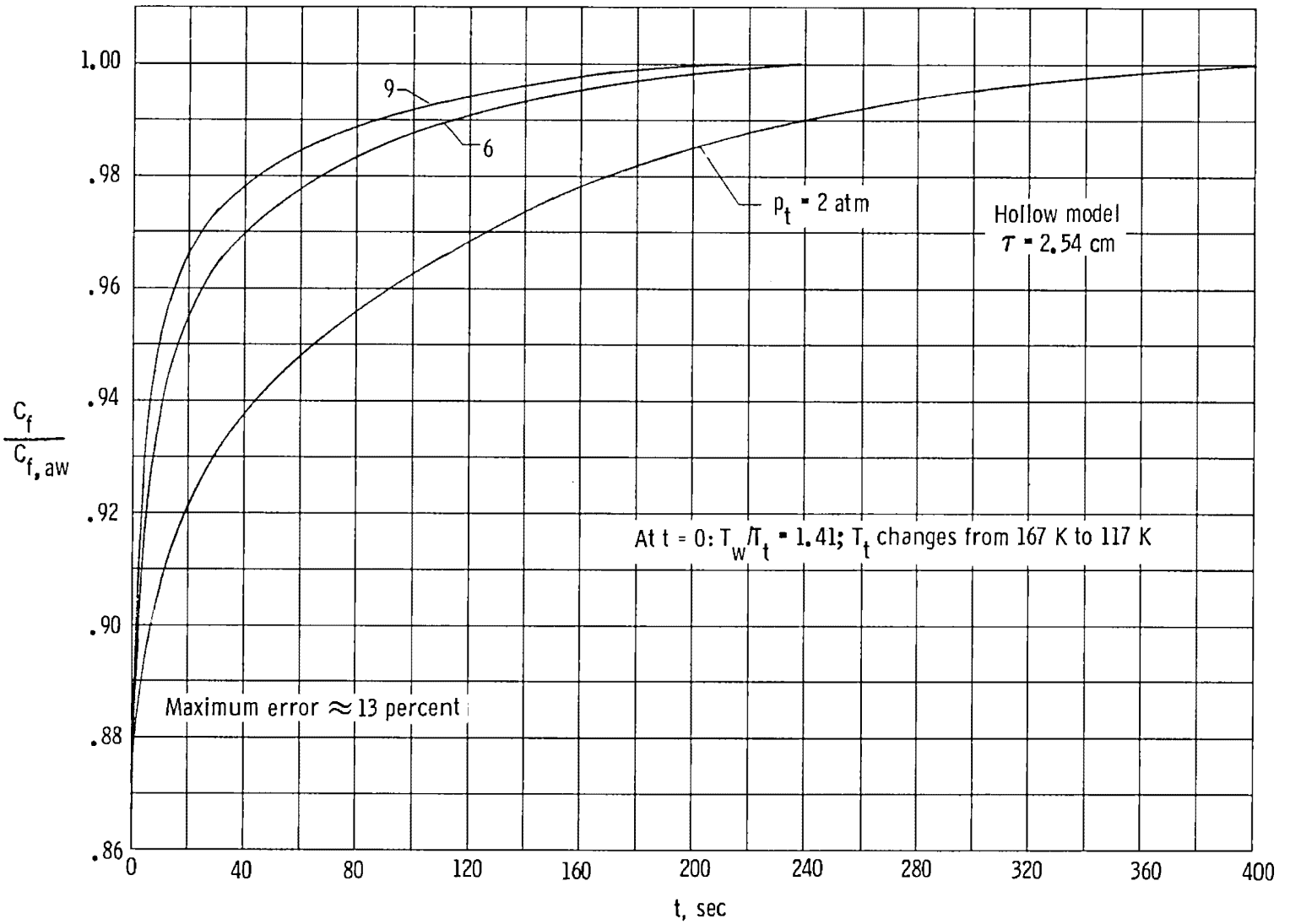

Figure 22.- Departure of C_f from $C_{f,aw}$ as a function of t for the NASA body of revolution at x/L = 0.5. L = 121.92 cm; M_∞ = 0.85.

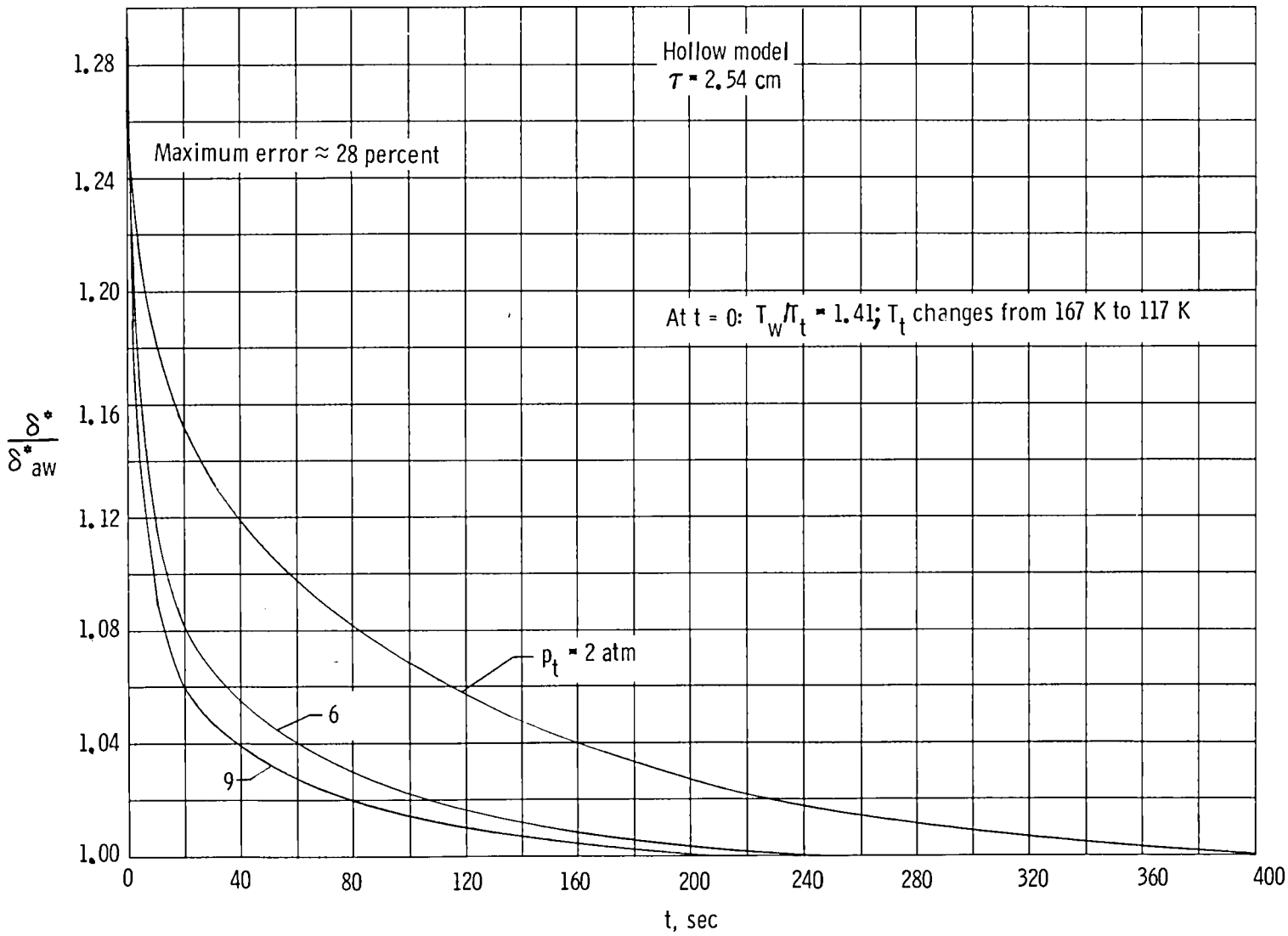

Figure 23.- Departure of δ^* from δ^*_{aw} as a function of t for the NASA body of revolution at x/L = 0.5. L = 121.92 cm; M_∞ = 0.85.

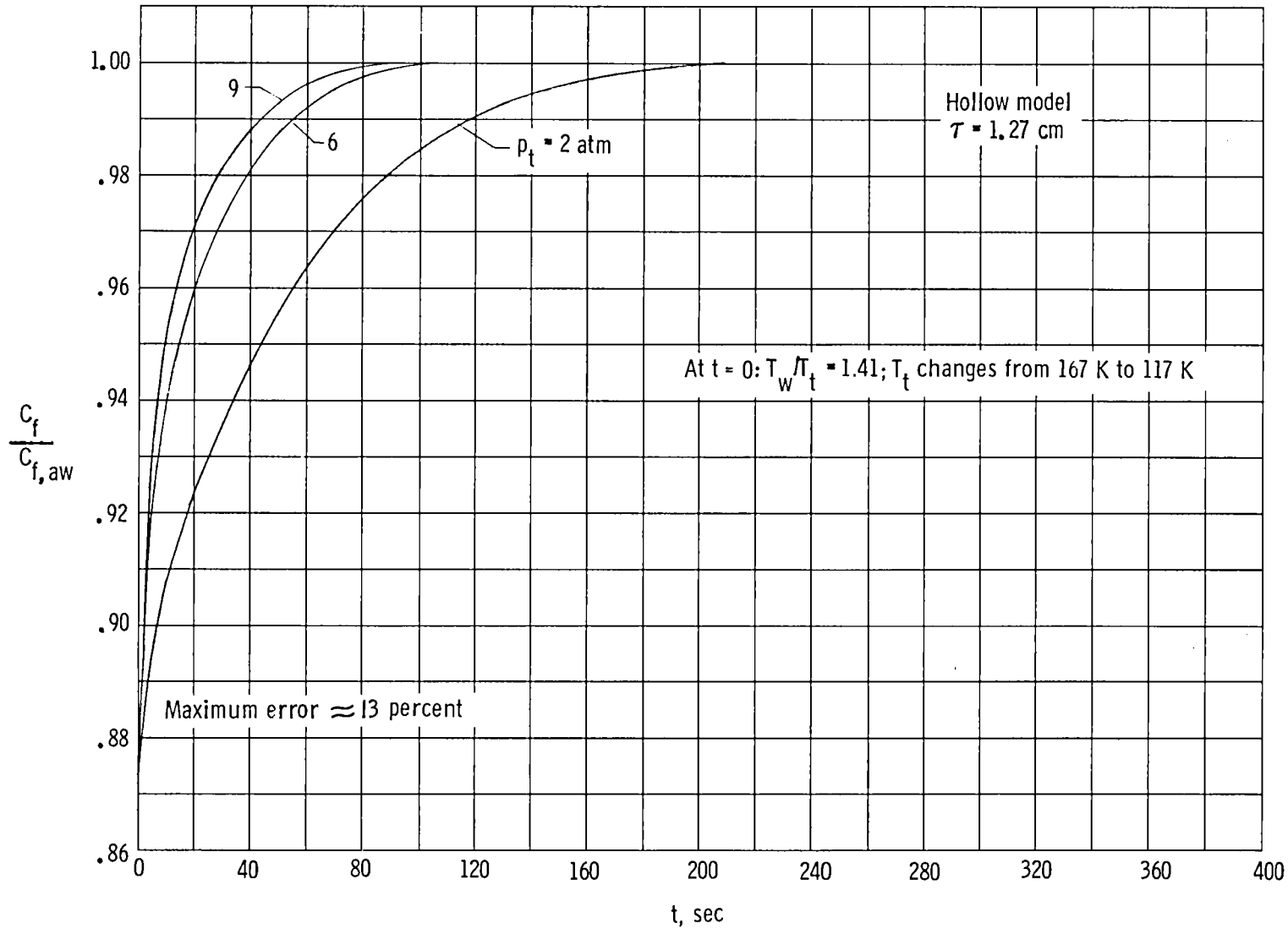

Figure 24.- Departure of C_f from $C_{f,aw}$ as a function of t for the NASA body of revolution at x/L = 0.5. L = 121.92 cm; M_∞ = 0.85.

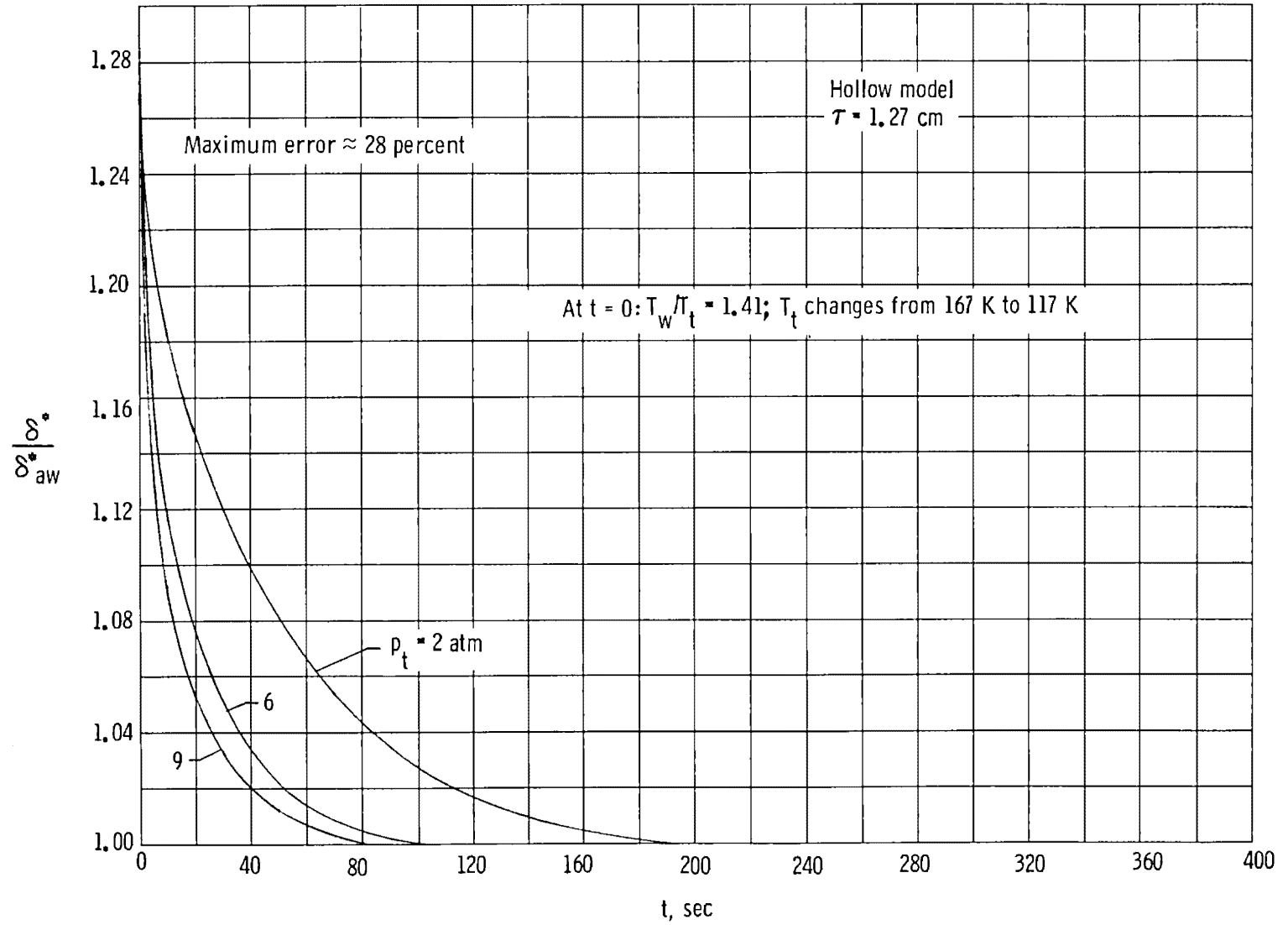

Figure 25.- Departure of δ^* from δ^*_{aw} as a function of t for the NASA body of revolution at x/L = 0.5. L = 121.92 cm; M_∞ = 0.85.

1. Report No.	2. Government Accession No.	3. Recipient's Catalog No.
NASA TM-80212		

4. Title and Subtitle	5. Report Date
THEORETICAL STUDY OF NONADIABATIC BOUNDARY-LAYER STABILIZATION TIMES IN A CRYOGENIC WIND TUNNEL FOR TYPICAL STAINLESS-STEEL WING AND FUSELAGE MODELS	July 1980
	6. Performing Organization Code

7. Author(s)	8. Performing Organization Report No.
Charles B. Johnson	L-13350
	10. Work Unit No. 505-31-53-01

9. Performing Organization Name and Address	11. Contract or Grant No.
NASA Langley Research Center Hampton, VA 23665	
	13. Type of Report and Period Covered Technical Memorandum

12. Sponsoring Agency Name and Address	14. Sponsoring Agency Code
National Aeronautics and Space Administration Washington, DC 20546	

15. Supplementary Notes

16. Abstract

A theoretical study has been made of the time-varying effect of nonadiabatic wall conditions on boundary-layer properties for a two-dimensional wing section and an axisymmetric fuselage. The wing and fuselage sections are representative of the wing root chord and fuselage of a typical transport model for the National Transonic Facility. The analysis was made with a solid wing and three fuselage configurations (one solid and two hollow with varying skin thicknesses) all made from AISI type 310S stainless steel. The displacement thickness and local skin friction were investigated at a station on the model in terms of the time required for these two boundary-layer properties to reach an adiabatic wall condition after a 50-K step change in total temperature. The analysis was made for a free-stream Mach number of 0.85, a total temperature of 117 K, and stagnation pressures of 2, 6, and 9 atm.

17. Key Words (Suggested by Author(s))	18. Distribution Statement
Cryogenic wind tunnel Model heat conduction Boundary layers Stabilization time	Unclassified - Unlimited Subject Category 34

19. Security Classif. (of this report)	20. Security Classif. (of this page)	21. No. of Pages	22. Price*
Unclassified	Unclassified	40	A03

For sale by the National Technical Information Service, Springfield, Virginia 22161

NASA-Langley, 1980

National Aeronautics and
Space Administration

Washington, D.C.
20546

Official Business
Penalty for Private Use, $300

SPECIAL FOURTH CLASS MAIL
BOOK

Postage and Fees Paid
National Aeronautics and
Space Administration
NASA-451

NASA

POSTMASTER: If Undeliverable (Section 158 Postal Manual) Do Not Return